[American Journal of Science, Vol. 310, December, 2010, P. 1421–1452, DOI 10.2475/10.2010.08]

THE ~390 Ma HIGH-*T* METAMORPHIC EVENT IN THE CHINESE ALTAI: A CONSEQUENCE OF RIDGE-SUBDUCTION?

YINGDE JIANG*, MIN SUN*,†, GUOCHUN ZHAO*, CHAO YUAN**, WENJIAO XIAO***, XIAOPING XIA*, XIAOPING LONG**, and FUYUAN WU***

ABSTRACT. High-grade rocks occur in the Chinese Altai, but the timing of metamorphism is poorly constrained, which hinders our understanding of the thermo-tectonic history of the region. Representative high-grade samples from the sillimanite zone extending from Hanas to Fuyun were selected for zircon U-Pb dating and temperature estimation. LA-ICP-MS analyses of zircon overgrowth rims and recrystallized domains give consistent ages of ~390 Ma, which is interpreted to record a regional metamorphic event. Temperature (*T*) estimations using the amphibole-plagioclase-quartz (Amp-Pl-Qtz) and garnet-biotite (GB) geothermometers give relatively high temperatures ranging from 650 to 700 °C. The zircon metamorphic rims yield temperature estimates of ~720 °C by using the Ti-in-zircon thermometer. These data suggest that a high-temperature metamorphic event took place in the Chinese Altai in the Middle Devonian, and may imply a tectonic environment involving an unusually elevated heat flux from a deep-seated source. Our data support possible ridge subduction around 390 Ma that caused upwelling of the hot asthenosphere and triggered the high-*T* metamorphism. This model can also account for coeval volcanic activity with a range of geochemical characteristics, diverse mafic intrusions and extensive hydrothermal mineralization in the Altai orogen.

Key words: Devonian, High-*T* metamorphism, ridge-subduction, Chinese Altai

INTRODUCTION

The Central Asian Orogenic Belt (CAOB), also referred to as the Altaids, extends from the Urals in the west to the Pacific in the east and from the Siberian and East European cratons in the north to the North China and Tarim cratons in the south (fig. 1, inset; Mossakovsky and others, 1993; Sengör and others, 1993; Jahn and others, 2000; Windley and others, 2007). It has a long evolutionary history from *ca.* 1.0 Ga (Khain and others, 2002) to *ca.* 250 Ma (Xiao and others, 2003) and consists of accreted geotectonic units including island arcs, ophiolites, accretionary prisms, seamounts and micro-continents, representing the world's largest region of juvenile crustal growth in the Phanerozoic (Jahn, 2004; Kovalenko and others, 2004; Kröner and others, 2007). Due to the diverse nature and different timing of the complicated amalgamation of these geotectonic units, controversy exists on the tectonic evolution of this orogenic belt. Its history has been interpreted using several competing models, including the syn-subduction strike-slip duplication and oroclinal bending of a single arc chain (Sengör and others, 1993; Sengör and Natal'in, 1996), and alternatively the amalgamation of unrelated arc terrains and continental blocks, a scenario similar to the modern western Pacific (Mossakovsky and others, 1993; Didenko and others, 1994; Windley and others, 2007; Xiao and others, 2009).

The Chinese Altai occupies a pivotal position in understanding the process of crustal growth in central Asia. However, its orogenic history, particularly in the early stage, has not been well studied. The traditional opening-closure model implied that a

* Department of Earth Sciences, The University of Hong Kong, Pokfulam Road, Hong Kong, China
** Key Laboratory of Isotope Geochronology and Geochemistry, Guangzhou Institute of Geochemistry, Chinese Academy of Sciences, Guangzhou 510640, China
*** State Key Laboratory of Lithospheric Evolution, Institute of Geology and Geophysics, Chinese Academy of Sciences, Beijing 100029, China
† Corresponding author: Min Sun, telephone (852) 28592194; fax: (852) 25176912; e-mail: minsun@hku.hk

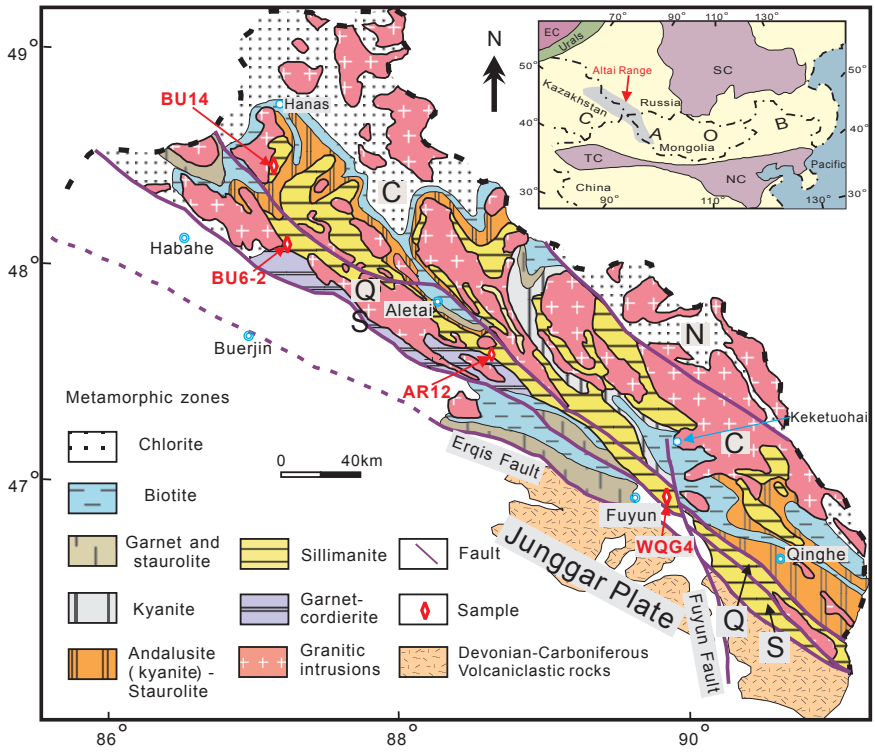

Fig. 1. Simplified geologic map of the Chinese Altai showing the main domains and distribution of metamorphic zones (modified from He and others, 1990; Zhuang, 1994; Li and others, 1996; Windley and others, 2002). N—North Altai Domain, C—Central Altai Domain, Q—Qiongkuer Domain, S—South Altai Domain. The inset shows the extent of the Central Asian Orogenic Belt (CAOB) and the location of the Altai Range. EC—East European Craton, SC—Siberia Craton, TC—Tarim Craton, NC—North China Craton.

Precambrian continent existed in the Chinese Altai region, and evolved as a passive continental margin during the Early Paleozoic (for example, He and others, 1990; Li and others, 2006). However, recent U-Pb dating of zircons from para- and orthogneisses gave Early Paleozoic ages, not Precambrian as expected (Wang and others, 2006; Briggs and others, 2007; Sun and others, 2008). These results suggest that Precambrian basement may not exist in the region. Instead, geochemical and zircon Hf isotopic data suggest that a complex subduction-accretion process was likely involved during the Early Paleozoic (Yuan and others, 2007; Long and others, 2008, 2010; Sun and others, 2009; Xiao and others, 2009).

Metamorphic rocks, with close genetic links to geodynamic events, can provide important constraints on major tectonic processes. A series of metamorphic zones are developed in the Chinese Altai and can be grouped as low-pressure (andalusite-sillimanite-cordierite) and medium-pressure (biotite-garnet-staurolite-kyanite) sequences (He and others, 1990; Zhuang, 1994; Zhang and others, 2004). On the basis of a re-evaluation of phase relations in the $K_2O+MnO+FeO+MgO+Al_2O_3+H_2O$ (KMnFMASH) and $K_2O+FeO+MgO+Al_2O_3+H_2O$ (KFMASH) systems, Wei and others (2007) and Zhang and others (2007) recently suggested that metamorphic zones in the Chinese Altai do not represent prograde evolution along a unique *P-T* array. The biotite, garnet, staurolite and kyanite zones mostly record a typical burial history, which is generally believed to be the

consequence of an arc-continent collision in the Late Paleozoic (Windley and others, 2002; Zhang and others, 2004) during the accretionary process. In contrast, the andalusite- and sillimanite-bearing zones represent a classic high-*T*/low-*P* metamorphic sequence, the tectonic significance of which, however, has been the subject of much controversy. It was speculated to result from either rifting (He and others, 1990) or from extensive intrusion of granites (Zhang and others, 2004), but no conclusive evidence has been provided. Typical high-*T*/low-*P* metamorphism commonly indicates high thermal gradients and is generally linked to tectonic environments of elevated heat flux driven by anomalously high heat flow and/or aqueous fluids (see review of De Yoreo and others, 1991). Such an environment has been reported throughout the world, for example, the Adelaide fold belt in southern Australia (Dymoke and Sandiford, 1992), the Hercynian massifs in Europe (Graeßner and Schenk, 1999), the Bushveld Complex in South Africa (Pitra and Waal, 2001), the Halls Creek Orogen in northern Australia (Bodorkos and others, 2002), the Trans-Hudson orogen in central Canada (White, 2005) and the Aracena metamorphic belt in SW Spain (Azpiroz and others, 2006). Since normal advection of heat by aqueous fluids is unlikely to produce high-*T*/low-*P* metamorphism (De Yoreo and others, 1991), additional heat from another source must play an important role. Thus, unraveling the mechanism of high-*T*/low-*P* metamorphic events can provide crucial clues for understanding the tectonic evolution of a region.

Although the *P-T* conditions of the high-*T* metamorphic event in the Chinese Altai have been evaluated in previous studies (Zhang and others, 2004, 2007; Wei and others, 2007), the timing of metamorphism has not been constrained, which strictly limits our understanding of its tectonic significance. Zircons from the high-grade rocks within the high-*T*/low-*P* metamorphic sequence commonly have a core-rim structure (Long and others, 2007; Sun and others, 2008). The zircon rims have low Th/U ratios and lack oscillatory zoning in cathodoluminescense (CL) images, suggesting they are metamorphic overgrowths and/or recrystallization features (see Hoskin and Black, 2000; Corfu and others, 2003). This paper reports results of U-Pb dating and Ti-in-zircon geothermometry on zircon rims from the high-grade metamorphic rocks of the Chinese Altai. Our data also shed light on the evolutionary history of the region.

GEOLOGICAL BACKGROUND AND SAMPLE DESCRIPTIONS

The NW-SE trending Altai orogen occupies the south-central part of the CAOB and extends for approximately 2500 km from Russia and East Kazakhstan in the west, through northern Xinjiang in China to southwestern Mongolia in the east (fig. 1, inset). Its Chinese segment (that is, the Chinese Altai) is divided into several domains (see fig. 1) that were named terranes by Windley and others (2002) and tectonostratigraphic units by Xiao and others (2004). The North Altai Domain (terrane 1 of Windley and others, 2002 and "N" in fig. 1) comprises Late Devonian–Early Carboniferous neritic clastic sedimentary rocks and limestones intercalated with minor island arc volcanic rocks, metamorphosed mostly at sub-greenschist facies. The Central Altai Domain (terranes 2 and 3 of Windley and others, 2002 and "C" in fig. 1) predominantly contains thick Middle Ordovician–Early Devonian turbiditic and pyroclastic sequences. These rocks are isoclinally folded with steep axial planes and metamorphosed at sub-greenschist to upper amphibolite facies. The Qiongkuer Domain (terrane 4 of Windley and others, 2002 and "Q" in fig. 1) consists mainly of Late Silurian to Early Devonian island arc-type lavas and pyroclastic rocks (Kangbutiebao Formation) in the lower part and a Middle Devonian turbiditic sand-shale sequence (Altai Formation) in the upper part. Rocks in this domain are metamorphosed from greenschist to upper amphibolite facies, and locally reach granulite facies. The South Altai Domain (terrane 5 of Windley and others, 2002 and "S" in fig. 1) includes a sequence of Devonian fossiliferous sediments and Late Carboniferous volcaniclastic

rocks, metamorphosed at greenschist to amphibolite facies. The Chinese Altai is separated from the Devonian-Carboniferous volcaniclastic rocks of the Junggar plate by the Erqis Fault, one of the largest transcurrent faults in central Asia (fig. 1). The 10-km-wide fault zone contains Devonian ophiolitic rocks (Wang and others, 2003) and was considered to be the site of Early to Middle Paleozoic subduction (Xiao and others, 2004), followed by large-scale (1000 km) sinistral displacement in the Late Paleozoic (290-280 Ma) (Laurent-Charvet and others, 2003). Some magnesian andesites, adakites, boninites, high-Ti basalts and Nb-rich basalts occur as tectonic blocks within the Devonian sediments along this fault zone (Xu and others, 2001, 2002; Zhang and others, 2003b, 2005; Niu and others, 2006a).

A series of metamorphic zones is identified within the Central Altai and Qiongkuer domains, passing from biotite, through garnet, staurolite, kyanite/staurolite-andalusite, to sillimanite, and locally, garnet-cordierite zones (fig. 1, Zhuang, 1994; Windley and others, 2002; Zhang and others, 2004, 2007; Wei and others, 2007). Detailed distribution of these metamorphic zones has been well documented by Zhuang (1994), Windley and others (2002) and Wei and others (2007), and they have been grouped into medium-*P* and high-T/low-P sequences. As a constituent component in high-*T*/low-*P* metamorphic sequence, the sillimanite zone extends from Hanas in the west to Qinghe in the east (fig. 1). Rocks in this zone mainly include amphibolites, banded gneisses and gneissic granitoids. Some gneisses are variably migmatized with prominently folded leucosomes (Long and others, 2007; Sun and others, 2008).

Four high-grade samples from the sillimanite zone were selected for this study to provide *P-T* estimations and age constraints for the high-*T*/low-*P* metamorphism mentioned above. Samples BU6-2 and BU14 were collected from the Habahe Group near the road between Buerjin and Hanas (fig. 1). Sample BU6-2 (lat. 48°03′17.8″N, long. 87°00′12.0″E) is a dark gray amphibolite, which is composed mostly of (in modal per cent) amphibole (45%), plagioclase (35%), biotite (15%) and minor amounts of quartz, epidote and opaque minerals (see fig. 2). Sample BU14 (lat. 48°19′14.8″N, long. 87°06′41.0″E) is a dark-gray coarse-grained paragneiss with alternating quartz-feldspar and biotite-amphibole bands. It consists mainly of quartz (40%), plagioclase (30%), K-feldspar (18%), biotite (10%) and minor sillimanite and blue-green amphibole (see fig. 2). Previous geochemical and geochronoloigical studies of sample BU14 demonstrated that it was originally derived from an immature sedimentary source and detrital zircons mostly gave Early Paleozoic and Neoproterozoic ages (Sun and others, 2008).

Samples AR12 and WQG4 were collected from the Qiongkuer Domain near Aletai and Fuyun cities, respectively. Sample AR12 (lat. 47°34′53.7″N, long. 88°25′11.3″E) is a medium-grained paragneiss consisting of quartz (55%), plagioclase (20%), biotite (15%), garnet (<5%), sillimanite (<5%), and minor amounts of ilmenite and magnetite (see fig. 2). Detrital zircons from this sample gave $^{206}Pb/^{238}U$ ages dominantly in the range of 456 Ma and 547 Ma, and some Neoproterozoic ages ranging from 553 Ma to 916 Ma (Long and others, 2007). Zircon rims yielded ~389 Ma $^{206}Pb/^{238}U$ ages, which were interpreted to be the metamorphic age, based on the low Th/U ratios (0.01-0.06, Long and others, 2007). Sample WQG4 (lat. 46°58′42.0″N, long. 89°40′49.2″E) is a dark gray granitic gneiss, with a strong fabric defined by biotite flakes. The rock is composed of quartz (35%), plagioclase (30%), K-feldspar (18%), biotite (12%) and muscovite (<5%) with a small amount of opaque minerals (mainly ilmenite). A granitic texture is apparent in thin section, and the plagioclase phenocrysts are surrounded by recrystallized, fine-grained quartz showing undulose extinction (fig. 2).

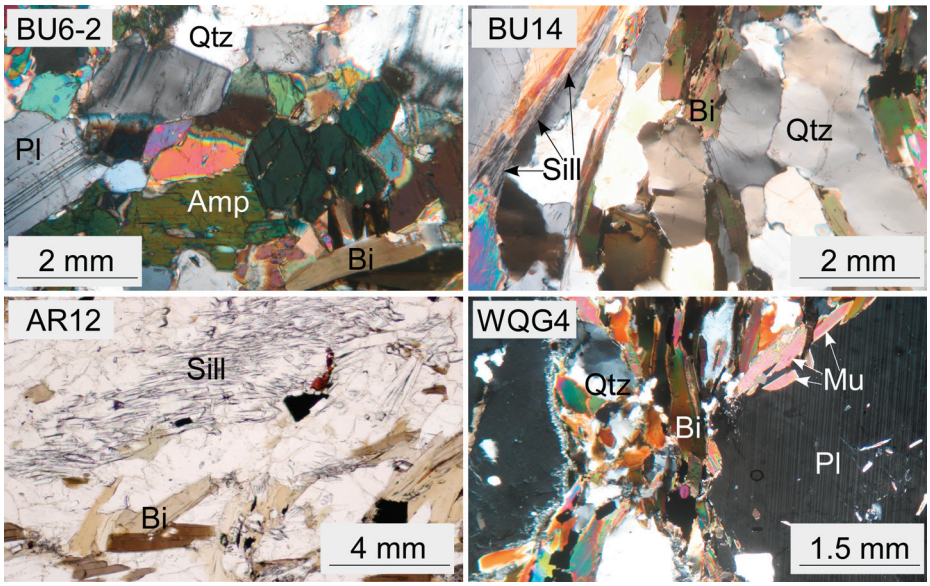

Fig. 2. Photomicrographs showing textural relationships in high-grade rocks from the sillimanite zone in the Chinese Altai. Amphibolite BU6-2 shows an equilibrium mineral assemblage of Amp+Pl+Bi+Qtz. In metapelitic samples BU14 and AR12, fibrous sillimanite crystals are aligned parallel to the principal foliation. Granitic gneiss WQG4 shows relict Pl phenocrysts surrounded by fine-grained recrystallized quartz. Photographs of BU6-2, BU14 and WQG4 were taken under cross-polarized light, and that of AR12 is under plane polarized light. Abbreviations for minerals: Pl—Plagioclase; Amp—amphibole; Bi—biotite; Sill—sillimanite; Qtz—quartz; Mu—muscovite.

ANALYTICAL METHODS

Mineral Chemistry

The chemical compositions of the constituent minerals were obtained using a JXA-8100 electron microprobe at the Guangzhou Institute of Geochemistry, Chinese Academy of Sciences (CAS). Analyses were conducted with 15 kV acceleration voltage, 20 nA beam current, 1–2 μm beam diameter and 20 s counting time. Matrix corrections were carried out using the ZAF correction procedure. Accuracy of the microprobe analyses was estimated to be ±2 percent.

Zircon Separation and CL Imaging

Zircons were separated by standard heavy liquid and magnetic techniques. Single grains were handpicked and mounted on adhesive tape, then enclosed in epoxy resin and polished to about half their size. After being photographed under reflected and transmitted light, the samples were prepared for CL imaging. CL images of the zircon grains were obtained using an electron microprobe (JXA-8100, JEOL) equipped with a Mono CL3 detector (Gatan) at the Guangzhou Institute of Geochemistry.

U-Pb Zircon Geochronology and Trace Element Determination

Zircon U-Pb isotopic analyses of samples BU6-2 and BU14 were carried out using a Nd:YAG 213 laser ablation system coupled with a VG PQ Excell ICP-MS at the Department of Earth Sciences, The University of Hong Kong, following the analytical procedure described by Xia and others (2004). During the analyses, highly purified helium was used as the carrier gas to improve the instrumental performance, and

zircon standard 91500 (1065 Ma, Wiedenbeck and others, 1995) was used for calibration.

In situ simultaneous determination of trace elements and U-Pb ages of sample AR12 and WQG4 were carried out using an Agilent 7500a Q-ICPMS and 193 nm laser ablation system installed at the Institute of Geology and Geophysics, CAS, Beijing. Spot sizes of 40 and 35 μm were applied to the cores and rims, respectively. ICP-MS measurements were carried out using time-resolved mode and peak hopping at one point per mass and dwell time for each isotope was set at 6ms for Si, Ti, Nb, Ta, Zr and REE, 15 ms for ^{204}Pb, ^{206}Pb, ^{207}Pb and ^{208}Pb and 10 ms for ^{232}Th and ^{238}U, respectively. Every 5 analyses were followed by one standard zircon 91500 and one NIST SRM 610 glass (Kane, 1998) measurement. Each spot analysis consists of 30 s background acquisition and 40 s data acquisition. More detailed instrumental settings and analytical procedures are described in Xie and others (2008).

The mass fractionation correction and isotopic results were calculated by GLITTER 4.0 (Macquarie University). A common Pb correction was applied to all the measured ratios using the interference and background corrected ^{204}Pb signal intensity using the model of Andersen (2002). The weighted mean U-Pb ages and concordia plots were processed using Isoplot 3.0 (Ludwig, 2003). Trace element concentrations were calculated using GLITTER 4.0, with ^{29}Si as an internal standard and NIST SRM 610 as an external reference material.

RESULTS

Structural Characteristics and Trace Element Composition of Zircons

Zircon grains from amphibolite sample BU6-2 are stubby to prismatic crystals with an average length to width ratio of 2:1. Some show concentric oscillatory zoning but with strongly corroded surfaces (fig. 3A), and they have Th/U ratios in the range of 0.17 to 2.24 (see table 1 and fig. 4A), suggesting an igneous origin (based on Hanchar and Rudnick, 1995). In contrast, others have similar Th/U ratios (0.61-1.93) but the original growth zoning is partly or completely replaced by nebulous and fir-tree sector zoning with slightly rounded terminations (figs. 3 B-D), a structure typically resulting from metamorphic recrystallization (Vavra and others, 1999; Huang and others, 2003; Gao and others, 2004; Wu and Zheng, 2004). A few zircon grains from this sample do have angular or corroded cores with low luminescence rims (figs. 3 E and F). Th/U ratios of these rims are comparatively low (~0.09, table 1 and fig. 4A), suggesting a metamorphic origin (Corfu and others, 2003; Hoskin and Schaltegger, 2003). Zircons in paragneiss samples BU14 and AR12 and granitic gneiss sample WQG4 are mostly euhedral to subhedral prisms, ranging from 0.1 mm to 0.2 mm in length with a length/width ratio <3:1. These grains commonly have a core-rim structure, that is, corroded, fragmented or rounded cores surrounded by weakly-zoned low-luminescent rims (figs. 3 G-S). Some cores have oscillatory zoning (figs. 3 G, H and P), but most cores have been apparently replaced by high or very low luminescent zircon that hardly reveals any internal structures (figs. 3 I-O and Q-S). There are also some high-luminescent zones around the cores, possibly indicating multi-stage growth (figs.3 J, K, M and O). The Th/U ratios of these cores vary from 0.1 to 1.4, mostly around 0.45 (table 1 and fig. 4A). Zircon rims, however, have much lower Th/U ratios which vary from 0.005 to 0.09, except for two points (table 1 and fig. 4A). The REE contents and some trace elements, such as Hf, P, Ti, Y and Ta, vary greatly between the zircon cores in samples AR12 and WQG4 (see table 2), which may possibly be due to a difference in the source rock types or the crystallization environments (Belousova and others, 2002). In contrast, the contents of these elements in zircon rims are similar, but commonly lower than those in the cores (table 2). The low Th/U ratios (<0.1) and relatively low total REE contents suggest a metamorphic origin for the low luminescent zircon rims

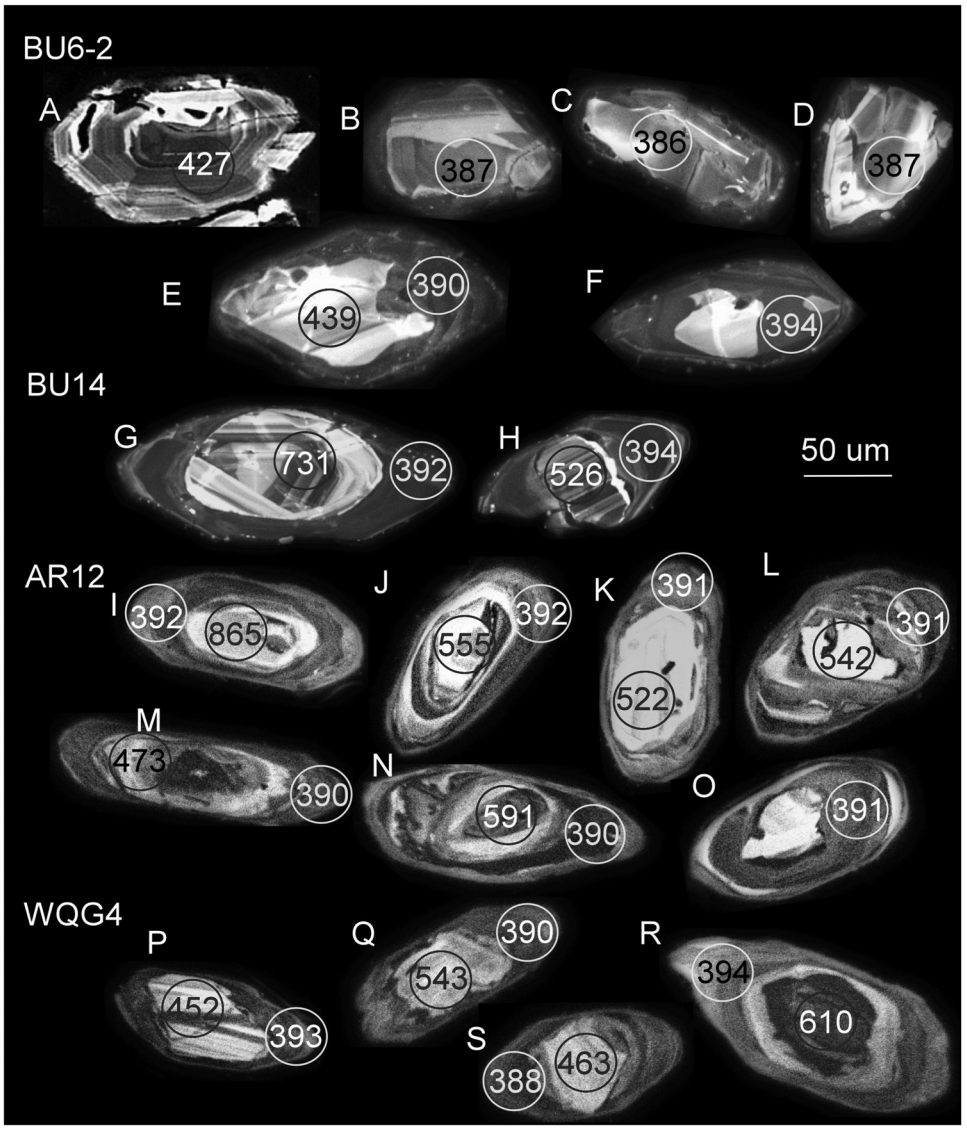

Fig. 3. Representative cathodoluminescence images for zircons from high-grade metamorphic rocks of the Chinese Altai. $^{206}Pb/^{238}U$ ages for zircon cores and rims are labeled at their respective analytical positions. The zircon grains in alphabetic order for sample BU6-2 are grains 26, 30, 31, 32, 23 and 33; for sample BU14 they are grains 7 and 14; for sample AR12 they are grains 5, 11, 14, 15, 18, 19 and 29; and for sample WQG4 they are grains 7, 13, 25 and 26. The full data are listed in table 1.

(Hoskin and Black, 2000; Corfu and others, 2003). The REE contents of zircon cores and rims from samples AR12 and WQG4 were normalized to chondrite values (Sun and McDonough, 1989), and are illustrated in figure 4. REE patterns obtained from zircon cores are characterized by positive Ce and negative Eu anomalies, and flat LREE but steep HREE patterns, typical of terrestrial igneous zircon (Hoskin and Schaltegger, 2003; Schulz and others, 2006). In the rims, the REE patterns show a positive Ce anomaly and a small negative Eu anomaly. LREE and MREE contents (from La to Gd)

Table 1

U-Pb data for zircons from high-grade metamorphic rocks in the Chinese Altai

Grain No.	Contents Th	U	Th/U	$^{207}Pb/^{206}Pb$	1σ	$^{207}Pb/^{235}U$	1σ	$^{206}Pb/^{238}U$	1σ	Age (Ma) $^{207}Pb/^{206}Pb$	1σ	$^{207}Pb/^{235}U$	1σ	$^{206}Pb/^{238}U$	1σ
BU6-2 (48°03′17.8″N, 87°00′12.0″E)															
Cores															
1	267	1037	0.26	0.05566	0.00112	0.53193	0.00988	0.06930	0.00121	439	19	433	7	432	7
2	249	202	1.23	0.05518	0.0013	0.51054	0.01123	0.06711	0.00120	420	22	419	8	419	7
3	157	163	0.97	0.05546	0.00135	0.53644	0.01221	0.07015	0.00126	431	23	436	8	437	8
4	175	205	0.86	0.05544	0.00127	0.51690	0.01099	0.06763	0.00120	430	21	423	7	422	7
5	120	80	1.51	0.05581	0.00163	0.53765	0.01480	0.06988	0.00129	445	31	437	10	435	8
6	82	195	0.42	0.05691	0.00132	0.53111	0.01145	0.06770	0.00120	488	22	433	8	422	7
7	375	203	1.85	0.05644	0.00260	0.54125	0.02397	0.06954	0.00148	470	61	439	16	433	9
8	115	96	1.19	0.05490	0.00169	0.51052	0.01494	0.06743	0.00125	408	34	419	10	421	8
9	65	70	0.92	0.05538	0.00145	0.52256	0.01284	0.06845	0.00123	428	26	427	9	427	7
10	301	441	0.68	0.05747	0.00130	0.53658	0.01126	0.06770	0.00119	510	21	436	7	422	7
11	90	355	0.25	0.05534	0.00124	0.51427	0.01071	0.06738	0.00118	426	21	421	7	420	7
12	412	228	1.80	0.05477	0.00134	0.51093	0.01164	0.06764	0.00120	403	24	419	8	422	7
13	96	224	0.43	0.05590	0.00162	0.52485	0.01426	0.06811	0.00125	448	30	428	9	425	8
14	60	67	0.89	0.05550	0.00208	0.52302	0.01865	0.06836	0.00133	432	46	427	12	426	8
15	150	870	0.17	0.05635	0.00123	0.52253	0.01038	0.06726	0.00117	466	20	427	7	420	7
16	206	422	0.49	0.05537	0.00126	0.52107	0.01097	0.06824	0.00120	427	21	426	7	426	7
17	592	363	1.63	0.05615	0.00147	0.57848	0.01401	0.07472	0.00133	458	26	463	9	465	8
18	88	96	0.91	0.05547	0.00187	0.51854	0.01645	0.06780	0.00128	431	38	424	11	423	8
19	446	199	2.24	0.05526	0.00145	0.51260	0.01237	0.06728	0.00119	423	26	420	8	420	7
20	139	119	1.17	0.05568	0.00225	0.53137	0.02041	0.06920	0.00138	440	51	433	14	431	8
21	558	465	1.20	0.05522	0.00139	0.51249	0.01176	0.06730	0.00118	421	24	420	8	420	7
22	108	159	0.68	0.05492	0.00378	0.51049	0.03426	0.06742	0.00169	409	105	419	23	421	10
23	673	486	1.39	0.05557	0.00174	0.53982	0.01654	0.07042	0.00142	435	35	438	11	439	9
24	182	658	0.28	0.05416	0.00155	0.51813	0.01452	0.06935	0.00138	378	31	424	10	432	8
25	111	193	0.57	0.05542	0.00189	0.52656	0.01750	0.06888	0.00141	429	39	430	12	429	9
26	104	415	0.25	0.05538	0.00130	0.52362	0.01209	0.06854	0.00134	428	23	428	8	427	8
27	324	847	0.38	0.06014	0.00180	0.82134	0.02399	0.09900	0.00200	609	31	609	13	609	12
28	53	143	0.37	0.06816	0.00147	1.36298	0.02897	0.14495	0.00282	873	20	873	12	873	16
29	11	54	0.20	0.05816	0.00393	0.67757	0.04453	0.08445	0.00214	536	99	525	27	523	13
Recrystallized grains & Rims															
30	121	112	1.08	0.05446	0.00183	0.46392	0.01485	0.06179	0.00117	390	73	387	10	387	7
31	260	428	0.61	0.05455	0.00131	0.46421	0.01012	0.06172	0.00108	394	53	387	7	386	7
32	247	128	1.93	0.05461	0.00181	0.47400	0.01472	0.06294	0.00118	392	59	388	8	387	7
26-r	80	905	0.09	0.05297	0.00121	0.45897	0.01034	0.06284	0.00122	389	53	390	7	390	7
33-r	109	616	0.18	0.05443	0.00132	0.46752	0.01023	0.06228	0.00109	396	72	394	10	394	7
BU14 (48°19′14.8″N, 87°06′41.0″E)															
Cores															
1	59	171	0.35	0.05873	0.00181	0.71068	0.02174	0.08776	0.00179	557	34	545	13	542	11
2	68	147	0.46	0.05807	0.00269	0.65224	0.02963	0.08146	0.00180	532	61	510	18	505	11
3	139	336	0.41	0.05964	0.00144	0.77013	0.01868	0.09365	0.00186	591	24	580	11	577	11
4	44	170	0.26	0.05899	0.00184	0.75119	0.02320	0.09236	0.00189	567	34	569	13	569	11
5	26	43	0.61	0.05844	0.00326	0.71406	0.03907	0.08861	0.00206	546	79	547	23	547	12
6	40	56	0.70	0.05879	0.00260	0.71367	0.03100	0.08804	0.00192	559	57	547	18	544	11
7	28	276	0.10	0.06379	0.00194	1.04179	0.03134	0.11844	0.00242	735	32	725	16	722	14
8	89	663	0.13	0.05811	0.00150	0.58421	0.01494	0.07290	0.00145	534	26	467	10	454	9
9	61	94	0.65	0.06436	0.00343	1.08626	0.05652	0.12239	0.00287	753	70	747	28	744	16
10	46	183	0.25	0.06199	0.00247	0.91845	0.03584	0.10744	0.00230	674	48	662	19	658	13
11	170	430	0.40	0.05617	0.00310	0.56396	0.03047	0.07281	0.00169	459	79	454	20	453	10
12	167	463	0.36	0.05733	0.00150	0.63860	0.01655	0.08078	0.00161	504	27	501	10	501	10
13	183	702	0.26	0.06507	0.00165	0.69440	0.01751	0.07739	0.00154	777	24	535	10	481	9
14	67	543	0.12	0.05773	0.00214	0.67621	0.02461	0.08494	0.00178	520	44	524	15	526	11
15	509	1133	0.45	0.05683	0.00286	0.57929	0.02845	0.07392	0.00164	485	69	464	18	460	10
16	65	444	0.15	0.05560	0.00229	0.54224	0.02184	0.07072	0.00148	436	53	440	14	440	9
17	49	118	0.42	0.05668	0.00162	0.59910	0.01681	0.07666	0.00151	479	30	477	11	476	9
18	56	247	0.22	0.05806	0.00172	0.59090	0.01722	0.07381	0.00146	532	32	471	11	459	9
Rims															
4-r	8	1144	0.07	0.05432	0.00471	0.45733	0.03976	0.06108	0.00132	384	158	382	28	382	8
7-r	18	280	0.07	0.05435	0.00213	0.46940	0.01809	0.06264	0.00132	386	50	391	13	392	8
11-r	69	823	0.08	0.05468	0.00529	0.47039	0.04581	0.06237	0.00144	399	178	391	32	390	9
14-r	32	347	0.09	0.07044	0.00130	0.61211	0.01096	0.06302	0.00066	941	73	485	14	394	8
17-r	69	1008	0.07	0.05522	0.00495	0.46717	0.04253	0.06130	0.00136	421	165	389	29	384	8

Table 1

(continued)

Grain No.	Contents Th	U	Ratios Th/U	$^{207}Pb/^{206}Pb$	1σ	$^{207}Pb/^{235}U$	1σ	$^{206}Pb/^{238}U$	1σ	Age (Ma) $^{207}Pb/^{206}Pb$	1σ	$^{207}Pb/^{235}U$	1σ	$^{206}Pb/^{238}U$	1σ
AR12 (47°34′53.7″N, 88°25′11.3″E)															
Cores															
1	170	445	0.38	0.05736	0.00131	0.64345	0.01342	0.08138	0.00115	505	23	504	8	504	7
2	31	246	0.13	0.05699	0.00321	0.62504	0.03231	0.07957	0.00219	491	67	493	20	494	13
3	338	1215	0.28	0.05795	0.00117	0.68058	0.01251	0.08521	0.00112	528	20	527	8	527	7
4	219	1644	0.13	0.05762	0.00116	0.66136	0.01210	0.08327	0.00110	515	19	515	7	516	7
5	69	317	0.22	0.06788	0.00193	1.34387	0.03490	0.14363	0.00245	865	28	865	15	865	14
6	829	2973	0.28	0.05664	0.00136	0.60410	0.01328	0.07738	0.00113	478	25	480	8	480	7
7	53	534	0.10	0.05677	0.00174	0.61035	0.01713	0.07800	0.00133	483	33	484	11	484	8
8	140	338	0.42	0.05733	0.00233	0.64874	0.02407	0.08210	0.00175	504	45	508	15	509	10
9	37	114	0.32	0.09723	0.00267	3.66137	0.09194	0.27320	0.00497	1572	23	1563	20	1557	25
10	364	928	0.39	0.06747	0.00160	1.31879	0.02844	0.14180	0.00214	852	22	854	12	855	12
11	73	197	0.37	0.05865	0.00182	0.72715	0.02061	0.08995	0.00158	554	33	555	12	555	9
12	130	343	0.38	0.05683	0.00186	0.60513	0.01803	0.07724	0.00140	485	35	480	11	480	8
13	25	125	0.20	0.05836	0.00212	0.70559	0.02339	0.08772	0.00171	543	40	542	14	542	10
14	115	325	0.36	0.05783	0.00228	0.67225	0.02413	0.08434	0.00177	523	43	522	15	522	11
15	72	225	0.32	0.05849	0.00219	0.70709	0.02412	0.08770	0.00178	548	41	543	14	542	11
16	11	135	0.08	0.12568	0.00346	6.45860	0.16262	0.37278	0.00688	2038	21	2040	22	2042	32
17	37	81	0.45	0.05835	0.00319	0.71038	0.03558	0.08831	0.00242	543	63	545	21	546	14
18	352	648	0.54	0.05658	0.00163	0.59358	0.01548	0.07610	0.00130	475	30	473	10	473	8
19	225	567	0.40	0.05962	0.00181	0.78892	0.02170	0.09598	0.00171	590	31	591	12	591	10
20	128	317	0.40	0.06739	0.00203	1.30957	0.03581	0.14095	0.00256	850	29	850	16	850	14
21	72	99	0.73	0.06418	0.00285	1.08953	0.04413	0.12313	0.00299	748	46	748	21	749	17
22	138	153	0.90	0.05710	0.00327	0.62648	0.03275	0.07958	0.00227	495	66	494	20	494	14
23	348	1753	0.20	0.05595	0.00176	0.55890	0.01588	0.07245	0.00134	450	32	451	10	451	8
24	27	530	0.05	0.06582	0.00221	1.20309	0.03659	0.13257	0.00262	801	33	802	17	803	15
25	176	668	0.26	0.05708	0.00185	0.62798	0.01841	0.07979	0.00152	495	33	495	11	495	9
26	80	1553	0.05	0.06157	0.00186	0.91468	0.02496	0.10774	0.00197	659	29	660	13	660	11
27	114	393	0.29	0.05957	0.00219	0.78694	0.02613	0.09580	0.00200	588	38	589	15	590	12
28	36	123	0.29	0.05763	0.00299	0.65925	0.03114	0.08296	0.00222	516	58	514	19	514	13
Rims															
5-r	32	468	0.07	0.05612	0.00193	0.48449	0.01524	0.06263	0.00114	457	39	401	10	392	7
11-r	35	483	0.07	0.05408	0.00156	0.46693	0.01225	0.06264	0.00104	374	31	389	8	392	6
14-r	7	449	0.01	0.05521	0.00246	0.47575	0.01931	0.06252	0.00141	421	52	395	13	391	9
15-r	4	544	0.01	0.05397	0.00178	0.46511	0.01394	0.06252	0.00114	370	36	388	10	391	7
18-r	96	467	0.21	0.05650	0.00174	0.48575	0.01358	0.06237	0.00111	472	32	402	9	390	7
19-r	18	491	0.04	0.05222	0.00179	0.44945	0.01399	0.06244	0.00118	295	38	377	10	390	7
29-r	16	389	0.04	0.05856	0.00286	0.50421	0.02243	0.06246	0.00154	551	55	415	15	391	9
WQG4 (46°58′42.0″N, 89°40′49.2″E)															
Cores															
1	95	199	0.48	0.05609	0.00479	0.57398	0.04677	0.07423	0.00226	456	127	461	30	462	14
2	115	186	0.62	0.05635	0.00795	0.56803	0.07637	0.07312	0.00361	466	211	457	49	455	22
3	210	346	0.61	0.05837	0.00282	0.70768	0.03258	0.08794	0.00170	544	67	543	19	543	10
4	164	267	0.61	0.05623	0.00306	0.57807	0.02996	0.07456	0.00154	461	78	463	19	464	9
5	316	440	0.72	0.05549	0.00710	0.54328	0.06631	0.07102	0.00317	432	193	441	44	442	19
6	103	372	0.28	0.05671	0.00395	0.60256	0.04004	0.07707	0.00197	480	102	479	25	479	12
7	275	681	0.40	0.05617	0.00250	0.56183	0.02380	0.07256	0.00130	459	62	453	15	452	8
8	113	542	0.21	0.08328	0.00109	2.32649	0.02749	0.20262	0.00224	1276	10	1220	8	1189	12
9	74	241	0.31	0.06767	0.00082	1.28492	0.01409	0.13772	0.00141	858	10	839	6	832	8
10	164	377	0.43	0.05807	0.00294	0.68295	0.03295	0.08530	0.00171	532	70	529	20	528	10
11	295	713	0.41	0.05674	0.00186	0.61206	0.01906	0.07824	0.00115	481	43	485	12	486	7
12	362	1194	0.30	0.06780	0.00048	1.29753	0.00816	0.13881	0.00124	862	9	845	4	838	7
13	294	1117	0.26	0.05849	0.00189	0.70816	0.02170	0.08783	0.00129	548	41	544	13	543	8
14	196	433	0.45	0.05628	0.00214	0.57691	0.02091	0.07436	0.00120	463	52	462	13	462	7
15	76	227	0.33	0.05613	0.00321	0.56439	0.03082	0.07294	0.00158	458	83	454	20	454	9
16	238	448	0.53	0.05790	0.00314	0.68840	0.03561	0.08625	0.00183	526	76	532	21	533	11
17	133	268	0.49	0.06654	0.00230	1.24119	0.04079	0.13530	0.00216	823	42	819	18	818	1
18	122	279	0.44	0.05863	0.00219	0.72012	0.02564	0.08910	0.00144	553	50	551	15	550	9
19	265	651	0.41	0.05601	0.00196	0.56209	0.01869	0.07280	0.00112	453	47	453	12	453	7
20	152	264	0.57	0.05865	0.00221	0.72393	0.02598	0.08955	0.00146	554	50	553	15	553	9
21	670	392	1.71	0.05624	0.00336	0.57912	0.03300	0.07470	0.00170	462	86	464	21	464	10
22	40	233	0.17	0.05642	0.00404	0.58325	0.03983	0.07499	0.00198	469	104	467	26	466	12
23	771	1201	0.64	0.05659	0.00181	0.58159	0.01772	0.07456	0.00111	476	41	465	11	464	7
24	682	1626	0.42	0.05593	0.00168	0.57240	0.0164	0.07424	0.00107	450	38	460	11	462	6
25	189	319	0.59	0.06010	0.00232	0.82270	0.03031	0.09930	0.00168	607	51	610	17	610	10

TABLE 1
(continued)

Grain No.	Contents Th	Contents U	Ratios Th/U	Ratios $^{207}Pb/^{206}Pb$	Ratios 1σ	Ratios $^{207}Pb/^{235}U$	Ratios 1σ	Ratios $^{206}Pb/^{238}U$	Ratios 1σ	Age (Ma) $^{207}Pb/^{206}Pb$	Age (Ma) 1σ	Age (Ma) $^{207}Pb/^{235}U$	Age (Ma) 1σ	Age (Ma) $^{206}Pb/^{238}U$	Age (Ma) 1σ
WQG4 (46°58′42.0″N, 89°40′49.2″E)															
Cores															
26	588	1191	0.49	0.05636	0.00275	0.57904	0.02691	0.07454	0.00146	467	68	464	17	463	9
27	224	1157	0.19	0.05690	0.00251	0.58723	0.02474	0.07487	0.00137	488	61	469	16	465	8
28	126	105	1.19	0.05611	0.00245	0.58026	0.02418	0.07502	0.00136	457	60	465	16	466	8
29	237	404	0.59	0.06536	0.00503	1.17404	0.08620	0.13030	0.00400	786	103	789	40	790	23
30	184	281	0.66	0.05656	0.00251	0.59720	0.02531	0.07661	0.00141	474	61	475	16	476	8
31	197	442	0.44	0.05719	0.00519	0.57899	0.05010	0.07344	0.00243	499	133	464	32	457	15
32	246	661	0.37	0.05573	0.00216	0.54956	0.02039	0.07153	0.00121	442	53	445	13	445	7
33	159	472	0.34	0.06725	0.00225	1.31162	0.04204	0.14148	0.00226	846	40	851	18	853	13
34	336	1311	0.26	0.06518	0.00370	1.17448	0.06368	0.13072	0.00309	780	74	789	30	792	18
35	280	299	0.94	0.06893	0.00213	1.38847	0.04108	0.14614	0.00222	897	36	884	17	879	12
36	13	51	0.25	0.05920	0.00391	0.75568	0.04766	0.09260	0.00237	574	93	572	28	571	14
37	197	278	0.71	0.05846	0.00305	0.69425	0.03333	0.08614	0.00218	547	62	535	20	533	13
38	204	363	0.56	0.05752	0.00284	0.65553	0.03092	0.08268	0.00167	512	68	512	19	512	10
39	116	524	0.22	0.06452	0.00308	1.03648	0.04732	0.11654	0.00239	759	62	722	24	711	14
40	283	451	0.63	0.06852	0.00237	1.38510	0.04591	0.14665	0.00242	884	42	883	20	882	14
41	94	269	0.35	0.05650	0.00265	0.58904	0.02645	0.07563	0.00148	472	65	470	17	470	9
42	170	325	0.52	0.06264	0.00317	0.97867	0.04734	0.11334	0.00241	696	67	693	24	692	14
43	207	446	0.46	0.05652	0.00306	0.58273	0.03019	0.07479	0.00162	473	76	466	19	465	10
44	190	512	0.37	0.26871	0.00248	22.8475	0.20223	0.61673	0.00696	3299	8	3220	9	3097	28
45	140	203	0.69	0.05811	0.00294	0.68912	0.03346	0.08603	0.00180	534	70	532	20	532	11
46	192	425	0.45	0.05830	0.00316	0.69976	0.03632	0.08707	0.00191	541	75	539	22	538	11
47	352	848	0.42	0.05650	0.00225	0.58556	0.02241	0.07518	0.00135	472	53	468	14	467	8
48	223	457	0.49	0.05699	0.00529	0.59320	0.05263	0.07551	0.00256	491	136	473	34	469	15
49	72	171	0.42	0.11135	0.00691	5.01968	0.30504	0.32712	0.00633	1822	82	1823	51	1824	31
50	56	170	0.33	0.05769	0.00453	0.6671	0.05175	0.08394	0.00162	518	137	519	32	520	10
Rims															
7-r	16	859	0.02	0.05442	0.00102	0.47114	0.00832	0.06280	0.00066	388	22	392	6	393	4
13-r	4	884	0.00	0.05459	0.00099	0.46943	0.00803	0.06237	0.00065	395	21	391	6	390	4
25-r	137	337	0.41	0.05497	0.00125	0.47757	0.01029	0.06303	0.00073	411	28	396	7	394	4
26-r	48	571	0.08	0.05468	0.00362	0.46721	0.02948	0.06199	0.00148	399	99	389	20	388	9
49-r	31	514	0.06	0.05495	0.00526	0.47277	0.04434	0.06242	0.00141	410	171	393	31	390	9
50-r	18	234	0.08	0.05949	0.00547	0.50690	0.04578	0.06185	0.0014	585	158	416	31	387	8
51-r	26	569	0.05	0.06036	0.00401	0.51718	0.00334	0.06211	0.00114	617	108	423	22	388	7

in zircon rims are lower than those of zircon cores, but the HREE patterns of the rims, are indistinguishable from those of the cores.

Zircon U-Pb Geochronology

The U-Pb isotopic data are presented in table 1 and shown on concordia diagrams in figure 5.

Amphibolite BU6-2.—Thirty-three zircon analyses were made, most on oscillatory zoned cores (for example, fig. 3A), with Th/U ratios ranging from 0.17 to 2.24 (see table 1 and fig. 4A), suggesting an igneous origin. Twenty-four analyses form a cluster with $^{206}Pb/^{238}U$ ages between 420 and 439 Ma and give a weighted mean age of 426 ± 3 Ma (table 1 and fig. 5A). We interpret this age as the age of magmatic crystallization of the protolith. Four other grains give $^{206}Pb/^{238}U$ ages of 465 ± 8, 523 ± 13, 609 ± 12 and 873 ± 16 Ma, and these are interpreted as xenocrysts.

Analyses on three recrystallized portions of grains yield $^{206}Pb/^{238}U$ ages of 387 ± 7, 386 ± 7 and 387 ± 7 Ma, respectively (table 1, figs. 3 B-D and fig. 5A). Two analyzed points on metamorphic rims have low Th/U ratios (0.18 and 0.09) and yield concordant results with $^{206}Pb/^{238}U$ ages of 394 ± 7 Ma and 390 ± 7 Ma, respectively (table 1,

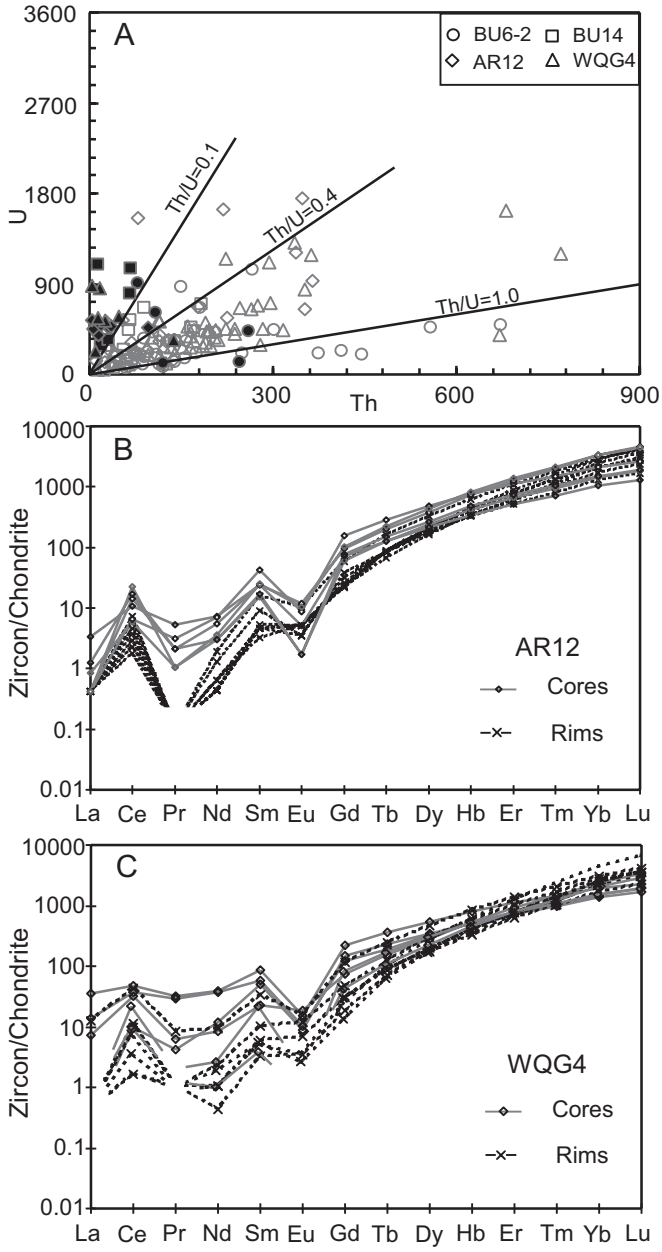

Fig. 4. (A) U-Th diagram for zircons from the high-grade metamorphic rocks of the Chinese Altai. Unfilled symbols in red represent the data from zircon cores and solid symbols in blue show the data from recrystallized domains and overgrowth rims. (B) and (C) chondrite-normalized REE patterns of zircon cores and metamorphic rims from samples AR12 and WQG4, respectively.

figs. 3 E-F, fig. 4A and fig. 5A). The above five analyses give a weighted mean $^{206}Pb/^{238}U$ age of 389 ± 6 Ma, taken to record the time of metamorphic crystallization/recrystallization.

TABLE 2

LA-ICP-MS trace element contents (ppm) of zircons from high-grade metamorphic rocks in the Chinese Altai

Sample	La	Ce	Pr	Nd	Sm	Eu	Gd	Tb	Dy	Ho	Er	Tm	Yb	Lu	REE	Hf*	Ta	P	Y	Nb	Ti	T°C†
											Cores											
AR12																						
1	4.9	24.6	2.3	13.7	8.2	1.2	26.0	9.2	108	40.9	191	43.0	431	81.4	985	0.97	1.2	1680	1182	2.9	19.6	
2	1.2	7.2	0.5	3.1	1.4	0.4	4.9	2.0	28.9	12.5	70.1	18.8	232	51.7	435	0.91	0.4	590	399	0.5	2.8	
3	0.3	15.0	0.3	3.2	8.1	0.3	42.9	17.1	204	77.1	329	65.9	611	106	1481	0.99	3.5	478	2175	8.9	23.5	
4	0.1	3.4	0.0	0.8	1.6	0.2	9.2	4.0	48.0	19.3	91.6	21.8	238	44.0	482	1.09	2.4	219	582	3.0	157	
5	0.2	3.6	0.1	1.4	2.3	0.1	12.3	4.7	59.9	24.0	110	24.2	243	46.5	533	0.97	0.6	374	699	1.1	6.4	
6	1.2	16.5	1.1	7.9	7.7	1.3	38.8	14.3	178	69.1	312	65.6	623	112.0	1449	0.95	4.3	556	1990	5.0	38.5	
7	0.1	3.8	0.0	0.3	0.7	0.3	5.4	3.3	52.2	24.1	130	32.7	361	69.7	684	0.94	1.0	542	726	1.4	19.6	
8	0.2	3.8	0.1	1.1	2.4	0.3	11.2	4.3	56.2	23.9	118	29.6	343	71.0	665	1.01	0.8	371	722	1.1	7.1	
9	1.7	12.3	0.8	4.4	4.8	0.7	23.1	8.4	102	39.0	174	38.2	365	66.9	841	1.01	0.9	290	1115	1.8	5.1	
10	0.4	12.0	0.3	2.7	3.9	0.6	23.9	9.7	124	47.9	225	49.2	505	95.0	1099	0.97	1.6	670	1419	3.0	3.4	
11	0.8	6.5	0.5	3.4	3.7	0.3	14.7	4.8	53.8	19.3	85.8	18.0	178	32.9	422	0.73	0.6	278	560	1.6	24.6	
12	1.8	15.0	0.9	7.5	6.4	0.5	22.6	7.4	84.4	31.7	142	29.8	282	53.6	685	0.81	0.7	573	902	2.1	5.1	
13	0.1	8.8	0.1	0.5	1.2	0.6	5.6	2.3	29.0	12.8	64.3	16.9	204	45.6	391	0.90	0.3	242	395	0.6	2.7	
14	0.1	4.0	0.3	3.3	6.4	0.5	32.2	10.6	122	43.7	188	38.1	361	66.4	876	0.87	0.8	119	1245	1.5	12.2	
15	0.1	8.7	0.2	2.6	3.7	0.7	19.6	7.5	96.8	41.5	206	50.4	577	119.0	1133	1.11	1.2	670	1233	2.1	4.5	
16	0.2	9.8	0.3	2.7	2.7	0.1	11.5	4.3	46.8	17.8	77.8	16.2	157	29.9	377	0.92	1.0	253	491	3.1	6.7	
17	3.7	9.3	0.9	3.7	1.4	0.3	3.7	1.6	20.5	6.9	24.1	3.9	32.6	5.9	119	1.23	1.0	107	220	1.8	5.0	
18	0.1	13.9	0.1	1.7	3.8	0.6	20.8	8.3	111	46.2	233	53.4	562	113.	1168	1.10	1.6	436	1377	3.9	9.0	
19	0.3	10.3	0.2	1.4	2.6	0.1	15.6	5.6	68.5	27.0	123	26.4	254	48.7	584	1.01	1.1	273	810	2.5	5.7	
20	0.1	2.3	0.2	3.3	6.7	0.2	36.8	13.9	167	63.3	278	58.7	558	103.0	1291	0.98	0.4	756	1813	0.7	6.2	
21	0.9	19.1	0.6	5.0	5.9	1.7	26.7	9.1	113	44.9	205	43.3	422	81.1	979	0.89	0.4	645	1249	0.9	5.1	
22	37.7	102.1	10.5	45.8	13.9	2.0	32.5	9.7	105	38.2	165	34.6	332	60.9	990	0.96	0.4	899	1140	0.9	5.7	
23	6.3	29.0	2.8	14.2	7.3	1.1	22.0	8.6	107	41.5	195	43.8	436	80.9	996	1.16	3.5	434	1231	4.3	5.2	
24	0.0	0.6	0.1	0.3	1.1	0.2	11.0	5.6	61.2	19.7	81.7	15.9	146	27.4	371	1.22	0.5	341	634	0.6	2.7	
25	0.2	7.9	0.1	1.2	2.3	0.2	11.8	4.3	52.4	19.9	93.5	20.5	201	39.1	455	0.91	1.1	289	601	1.7	2.9	
36	0.2	3.1	0.2	1.2	1.3	0.6	5.8	2.7	47.4	20.2	119	29.3	343	73.0	647	1.25	6.6	389	653	7.0	11.3	
27	9.7	40.1	3.6	19.5	11.0	0.3	42.4	16.3	199	79.1	344	67.8	629	116.4	1578	0.93	1.0	467	2099	3.1	3.3	
28	0.1	10.5	0.2	2.3	3.6	1.9	14.8	4.8	55.3	20.7	94.4	21.8	226	47.5	504	0.84	0.3	248	619	0.5	7.6	
WQG4																						
1	-	16.4	0.1	2.2	3.7	1.4	24.8	8.6	109	42.8	204	44.3	456	87.0	1000	0.88	0.7	501	1277	2.4	12.5	
2	2.0	33.9	0.7	5.6	4.6	1.8	19.7	6.5	75.0	30.0	137	30.8	326	65.6	739	0.73	0.6	376	899	2.3	9.9	
3	-	5.2	0.2	2.6	4.3	0.4	16.8	6.1	70.0	26.3	124	26.0	254	48.7	584	0.74	0.4	329	865	0.7	31.5	
4	3.5	22.0	1.1	8.0	6.2	1.0	23.3	7.3	76.6	28.3	127	27.0	266	51.6	649	0.71	0.6	252	874	1.4	5.6	
5	0.1	24.6	0.3	3.5	5.7	1.4	33.1	12.6	165	67.1	323	70.7	732	141.2	1580	1.02	1.2	447	2021	3.5	14.0	
6	0.1	13.8	0.1	1.5	3.0	0.6	13.7	4.7	58.3	23.4	112	26.6	287	57.4	602	1.01	0.8	329	736	1.0	8.3	
7	8.2	29.6	3.0	17.8	13.1	0.9	44.4	13.4	139	46.1	186	36.4	329	57.8	925	0.96	0.7	627	1325	1.5	9.8	
8	0.0	6.0	0.0	0.5	1.0	0.3	5.2	2.2	25.0	9.9	47.4	11.0	123	23.9	255	1.18	0.4	153	323	0.7	4.8	
9	1.6	25.3	0.4	2.6	2.8	0.7	10.8	3.6	47.1	18.9	90.8	21.3	234	45.5	506	1.06	0.8	312	594	1.6	16.9	
10	4.4	31.1	1.0	5.5	2.9	0.8	11.7	4.3	49.2	19.7	93.7	22.4	242	53.1	542	0.97	0.5	599	645	1.2	4.4	

Table 2
(continued)

Sample	La	Ce	Pr	Nd	Sm	Eu	Gd	Tb	Dy	Ho	Er	Tm	Yb	Lu	REE	Hf*	Ta	P	Y	Nb	Ti	T°C†
											Cores											
WQG4																						
11	0.2	18.5	0.4	4.3	8.2	0.8	37.6	14.5	169	63.6	283	58.8	544	98.8	1302	1.05	2.1	372	1907	5.7	15.4	
12	0.7	11.0	0.4	3.0	4.4	0.3	26.7	10.3	134	53.2	246	51.6	506	94.4	1142	1.18	1.4	475	1551	3.5	7.5	
13	3.3	22.5	2.7	17.3	8.9	0.6	24.9	7.1	83.2	28.7	126	27.0	264	48.4	664	1.07	1.4	1809	885	2.1	6.1	
14	5.9	44.3	1.6	9.0	6.0	2.2	23.1	7.0	78.5	28.6	128	29.5	300	61.3	725	0.92	0.3	719	906	1.2	8.7	
15	0.4	9.1	0.2	1.9	3.3	0.4	17.1	6.4	81.6	31.1	142	29.0	284	53.0	659	0.90	1.0	292	920	2.6	53.0	
16	0.6	20.8	0.3	2.6	3.5	0.5	18.8	7.1	90.7	37.5	172	37.7	375	70.9	837	1.04	2.0	289	1078	6.1	332	
17	-	11.6	0.2	3.1	6.5	0.5	30.1	11.3	133	50.0	230	48.5	467	85.6	1078	1.01	1.0	550	1491	2.0	19.8	
18	0.1	17.6	0.3	6.5	13.0	3.0	55.7	18.1	201	70.5	295	59.5	549	96.7	1385	0.69	1.8	184	2034	4.9	3.5	
19	0.2	11.3	0.5	6.6	6.9	0.7	27.3	8.3	90.6	31.3	136	27.5	267	51.0	665	0.93	0.8	553	933	1.8	13.3	
20	-	15.8	0.1	2.1	2.9	0.7	14.4	4.9	60.8	24.8	123	29.2	320	67.6	667	1.08	0.5	161	759	1.0	6.1	
21	0.1	13.8	0.6	9.5	18.6	0.9	79.2	25.4	270	94.2	384	73.6	661	115	1747	1.04	1.2	343	2672	3.6	160	
22	5.5	20.7	1.6	8.4	4.8	0.8	18.9	6.9	90.6	38.0	180	40.6	411	82.1	910	0.92	0.5	550	1143	1.1	5.8	
23	0.1	45.9	0.2	3.8	6.0	1.6	30.1	10.7	136	52.9	241	51.8	514	98.6	1193	0.90	1.3	310	1597	4.2	8.3	
24	11.9	44.8	3.4	18.3	10.9	0.5	48.2	17.6	208	80.4	346	69.3	652	117	1629	1.07	3.8	499	2240	7.8	12.6	
25	1.7	19.7	0.6	4.0	3.4	1.1	15.5	5.9	73.1	30.9	153	37.1	404	86.6	836	1.03	1.1	360	957	3.2	13.3	
26	0.1	6.0	0.4	5.6	7.5	0.5	30.0	8.6	86.3	29.0	118	24.4	232	43.3	592	1.06	0.7	181	910	1.1	27.5	
27	0.3	11.6	0.3	2.7	3.8	0.6	16.0	6.5	79.2	29.7	140	32.2	341	63.0	727	1.17	1.5	302	908	2.3	22.8	
28	0.1	40.3	0.2	2.5	4.5	0.9	18.4	6.1	72.8	27.8	131	28.8	303	61.0	697	0.96	0.9	215	845	2.5	13.7	
29	0.0	18.6	0.3	4.6	6.3	1.4	22.1	6.7	75.4	29.1	132	27.7	274	55.1	654	0.85	0.4	213	881	0.7	12.4	
30	6.0	28.7	1.3	5.4	2.5	0.6	8.9	3.2	41.6	17.3	90.4	22.6	260	56.3	545	0.99	0.6	500	569	1.3	14.5	
31	0.1	34.1	0.1	1.4	1.9	0.9	11.0	4.6	60.4	25.7	121	28.3	305	60.0	654	0.84	1.1	39.4	755	3.0	4.4	
32	0.1	12.3	0.2	2.8	5.4	1.3	26.9	9.6	114	44.7	203	44.4	442	86.3	993	0.93	0.7	286	1342	1.7	8.0	
33	1.2	8.6	0.7	6.9	10.7	1.1	45.1	16.0	193	74.2	330	66.5	618	111	1483	1.05	1.0	549	2079	2.3	18.6	
34	1.6	34.8	0.6	4.1	3.6	0.6	18.7	7.6	103	43.1	217	50.8	524	108	1118	1.15	5.8	626	1341	5.3	25.1	
35	1.5	13.0	0.6	3.6	3.1	0.2	17.1	6.3	79.4	31.2	144	31.2	303	57.1	692	0.98	1.7	307	927	3.6	9.6	
36	-	18.1	0.3	4.8	7.7	1.4	34.6	11.9	135	51.6	228	46.0	429	81.6	1050	1.02	0.4	284	1530	0.9	11.3	
37	0.0	3.0	0.0	0.4	1.0	0.4	5.0	2.2	26.3	11.6	61.1	14.9	169	41.2	336	0.88	0.1	177	376	0.1	6.3	
38	15.6	55.3	4.2	18.3	5.3	1.0	16.1	4.9	58.9	23.0	106	23.8	244	50.9	627	0.95	0.6	854	687	1.1	5.1	
39	0.1	30.4	0.1	1.9	3.3	1.3	15.6	5.5	67.8	26.4	125	28.8	305	63.8	675	1.04	0.9	244	836	2.9	3.3	
40	0.8	4.9	0.3	2.6	4.6	0.2	24.7	10.0	125	49.9	218	44.3	413	76.1	975	1.10	0.8	402	1396	1.2	6.1	
41	4.0	43.2	1.2	7.2	6.1	1.1	23.5	7.5	90.4	34.1	158	34.4	345	65.2	821	0.92	0.9	574	1034	2.0	8.1	
42	-	17.8	0.1	1.9	2.8	1.3	13.5	5.0	61.3	24.7	120	28.3	297	62.9	636	0.86	0.4	228	743	1.2	17.7	
43	1.5	24.9	0.4	2.8	2.5	0.8	10.4	3.6	43.7	17.7	85.4	20.0	222	46.5	482	0.81	0.5	251	564	1.6	145	
44	0.1	14.5	0.1	2.6	6.7	0.8	39.2	14.8	191	74.7	328	63.2	564	98.1	1398	0.89	2.6	320	2097	7.2	93.5	
45	17.3	52.1	5.3	24.4	7.0	1.1	18.8	6.6	79.1	32.4	155	36.5	378	76.9	891	1.01	1.2	1144	972	2.2	5.2	
46	-	17.8	0.3	4.6	7.9	2.5	41.0	13.9	153	55.9	244	51.0	469	90.2	1151	0.73	0.1	242	1674	0.6	12.9	
47	0.5	10.2	0.4	4.4	5.1	0.6	17.2	5.2	55.5	19.1	82.5	17.4	171	32.0	421	0.95	0.9	258	598	1.3	28.7	
48	0.4	13.3	0.3	3.9	5.6	0.5	29.2	10.2	130	49.8	228	49.6	462	85.6	1068	0.92	1.0	278	1360	3.0	3.1	
49	-	13.2	-	1.3	3.3	-	16.4	6.0	72.9	28.1	121	25.7	242	44.5	575	1.00	2.4	177	773	8.2	7.2	
50	-	6.0	-	0.5	0.6	-	8.5	3.9	53.9	24.3	122	29.2	323	67.2	693	0.98	0.88	145	396	1.2	3.3	

TABLE 2
(continued)

Sample	La	Ce	Pr	Nd	Sm	Eu	Gd	Tb	Dy	Ho	Er	Tm	Yb	Lu	REE	Hf*	Ta	P	Y	Nb	Ti	T°C†
											Rims											
AR12																						
5-r	0.1	1.4	0.0	0.2	0.7	0.2	6.6	3.1	44.5	18.4	86.4	19.9	220	42.6	444	1.08	0.8	355	561	1.0	3.3	674
11-r	0.0	2.8	0.0	0.6	1.4	0.2	7.8	3.1	47.2	19.5	100	25.6	292	60.6	561	1.04	1.1	346	589	1.4	8.6	759
14-r	0.0	2.3	0.0	0.2	0.8	0.3	4.6	2.5	41.4	19.2	103	28.5	348	75.8	627	1.16	0.9	448	590	0.8	3.7	684
15-r	0.0	1.1	0.0	0.2	0.7	0.3	4.8	3.1	50.2	22.5	120	34.5	419	90.3	746	1.21	1.1	610	688	0.9	3.7	684
18-r	0.0	4.5	0.1	0.9	2.4	0.6	12.1	6.0	82.4	35.0	183	45.2	499	101	972	1.15	1.4	565	1060	1.6	6.6	734
19-r	0.0	1.8	0.0	0.3	0.5	0.3	4.5	3.2	52.9	25.6	144	39.1	470	104	846	1.28	1.0	608	778	1.4	11.7	789
29-r	0.1	3.8	0.0	0.3	0.7	0.3	5.4	3.3	52.2	24.1	130	32.7	361	69.7	684	0.94	1.0	371	722	1.1	7.1	740
WQG4																						
7-r	0.1	7.0	0.1	1.1	1.6	0.7	10.0	4.6	75.7	33.6	171	42.5	461	89.8	899	1.11	1.7	709	1032	1.4	9.8	772
13-r	-	1.0	-	0.2	0.5	0.2	3.9	2.7	43.4	19.0	103	26.0	284	56.5	540	0.00	0.0	455	617	0.9	3.2	673
25-r	2.9	26.5	0.8	4.3	5.2	0.9	24.2	9.3	117.4	47.9	229	51.6	521	102	1143	1.06	0.8	435	1408	1.9	4.6	702
26-r	-	6.1	0.1	0.5	0.9	0.4	6.3	3.3	49.8	23.2	129	34.6	422	88.5	765	0.00	0.1	437	710	1.3	10.3	776
49-r	-	4.7	-	0.91	0.9	0.2	2.8	2.3	41.5	19.4	108	28.6	335	70.6	614	1.16	2.0	457	652	4.3	4.6	702
50-r	-	2.2	-	0.5	-	-	6.0	3.3	45.7	22.3	119	32.8	388	86.2	707	0.91	0.6	763	655	0.6	3.8	685
51-r	-	1.1	-	-	0.8	0.2	5.0	3.7	66.7	33	195	56.5	698	157	1217	1.35	1.15	526	1083	3.9	4.8	705

* Hf concentrations are given in wt%.
† T °C calculated using the Ferry and Watson (2007) calibration.

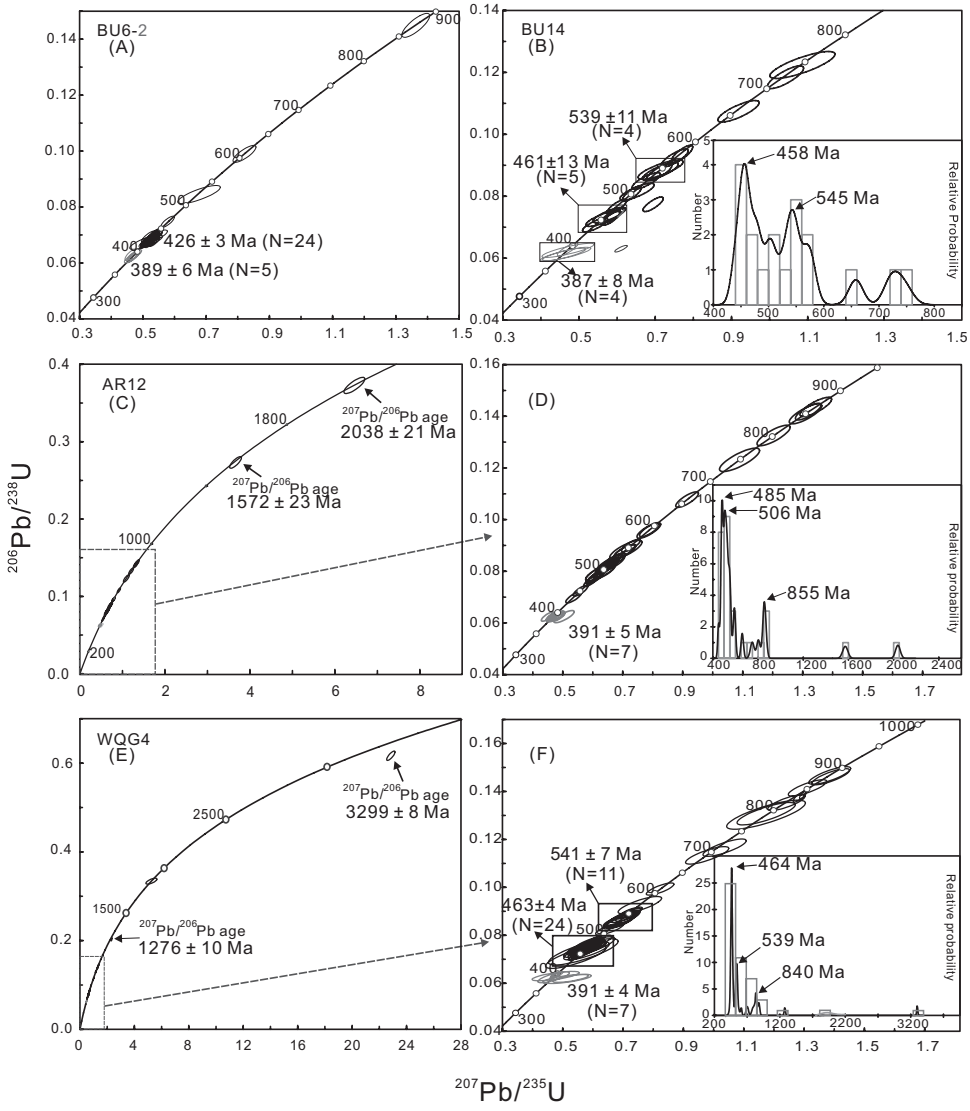

Fig. 5. U-Pb concordia diagrams for zircons from the high-grade metamorphic rocks of the Chinese Altai. The analyses of zircon cores are shown by red error ellipses, whereas those on metamorphic overgrowth zircon rims and grains devoid of zoning are shown by blue error ellipses. The insets are histograms showing the distribution of $^{206}Pb/^{238}U$ and $^{207}Pb/^{206}Pb$ ages for zircons younger than 1.0 Ga and older than 1.0 Ga, respectively.

Paragneiss BU14.—Eighteen zircon grains with core-rim structure were selected for U-Pb isotopic analyses. Most of the zircon cores possess Th/U ratios between 0.1 and 0.7 (table 1 and fig. 4A) and give $^{206}Pb/^{238}U$ ages between 440 and 577 Ma, with a prominent peak at 458 Ma and a minor peak at 545 Ma, corresponding to weighted mean $^{206}Pb/^{238}U$ ages of 461 ± 13 and 539 ± 11 Ma, respectively. Other cores give slightly older Neoproterozoic $^{206}Pb/^{238}U$ ages ranging from 658 to 744 Ma (table 1 and fig. 5B).

Four zircon rims have Th/U ratios of 0.07 to 0.08, and yield $^{206}Pb/^{238}U$ ages between 382 and 392 Ma with a weighted mean age of 387 ± 8 Ma (table 1 and fig. 5B).

Paragneiss AR12.—Twenty-nine zircon grains were selected for U-Pb isotopic analyses. Many zircon cores have similar Th/U ratios between 0.2 and 0.4 (table 1 and fig. 4A), and give $^{206}Pb/^{238}U$ ages ranging between 451 Ma and 591 Ma, with a prominent peak at 485 Ma, and a slightly older peak at 506 Ma (table 1 and figs. 5 C and D). Other cores have Th/U ratios from 0.05 to 0.73 and give older ages ranging from Paleoproterozoic to Neoproterozoic with a small peak at 855 Ma (table 1, fig. 4A and figs. 5 C and D). U-Pb isotopic analyses on the rims of seven zircon grains (figs. 3 I-O) give Th/U ratios varying from 0.01 to 0.07, except for one of 0.21 (table 1 and fig. 4A), and yield $^{206}Pb/^{238}U$ ages between 390 and 392 Ma and a weighted mean age of 391 ± 5 Ma (table 1 and figs. 5 C and D).

Granitic gneiss WGQ4.—Fifty-one zircon grains from this sample were analyzed for U-Pb isotopic compositions. Twenty-four analyses on the corroded cores have Th/U ratios between 0.17 and 1.71 (avg. 0.53), and form a tight cluster of concordant points, giving a weighted mean $^{206}Pb/^{238}U$ age of 463 ± 4 Ma. A further eleven analyses on the corroded cores, with Th/U ratios from 0.25 to 0.71 (avg. 0.50), yield $^{206}Pb/^{238}U$ ages between 512 and 571 Ma, with a peak at 539 Ma and a weighted mean $^{206}Pb/^{238}U$ age of 541 ± 7 Ma. Twelve additional analyses on the cores have Th/U ratios from 0.22 to 0.94 and give Neoproterozoic $^{206}Pb/^{238}U$ ages between 610 and 882 Ma. Moreover, two analyses yield concordant $^{207}Pb/^{206}Pb$ ages of ~1.28 and ~1.82 Ga and one slightly discordant analysis yields a $^{207}Pb/^{206}Pb$ age of 3299 ± 8 Ma (table 1 and figs. 5 E and F).

Seven zircon rims were analyzed and six yield very low Th/U ratios between 0.005 and 0.08, except for one of 0.41 (see table 1 and fig. 4A). These analyses give $^{206}Pb/^{238}U$ ages ranging between 387 and 394 Ma, with a weighted mean $^{206}Pb/^{238}U$ age of 391 ± 4 Ma (table 1 and figs. 5 E and F).

P-T Estimation

Sample BU6-2 has a mineral assemblage of amphibole, plagioclase and biotite, indicating amphibolite facies metamorphic conditions. Minerals in the metapelitic sample AR12 include sillimanite, garnet, biotite, plagioclase and quartz, indicating that the rock was metamorphosed at middle to upper amphibolite facies. The mineral assemblages of amphibole-plagioclase-quartz and garnet-biotite-plagioclase-quartz in the two samples are suitable for geothermobarmetric study. The chemical compositions of selected minerals and results of *P-T* estimations are presented in table 3.

Plagioclase in sample BU6-2 has a composition of An_{45-60} and the brown-green amphibole in this sample belongs to the calcic series and can be further classified as magnesiohornblende (Leake and others, 1997). Each mineral in this sample is in sharp contact with other minerals and no obvious reaction or disequilibrium textures, such as coronas or symplectites, are recognized (see fig. 2), suggesting an equilibrium mineral assemblage. Using the Amp-Pl-Qtz thermometer of Holland and Blundy (1994), which is based on the NaAl = Si exchange between amphibole and quartz and NaSi = CaAl exchange between amphibole and plagioclase, the temperature is estimated at ~652°C. Garnet porphyroblasts from sample AR12 have poorly preserved compositional zoning with a smooth increase in Fe/(Fe+Mg) and Mn from the core toward the rim (table 3 and fig. 6), and biotite in the matrix near garnet commonly has Fe/(Fe+Mg) values higher than that farther from garnet grains. This suggests that the garnet grains may have been affected by retrograde net transfer reactions (see summary in Kohn and Spear, 2000). As a result, the garnet dissolution may enrich biotite in Fe, and then, when pairing the garnet with biotite for *T* estimation, may cause calculated temperatures higher than peak conditions (Spear, 1991; Spear and Flor-

TABLE 3

Microprobe analyses of selected minerals from high-grade metamorphic rocks in the Chinese Altai

Sample	AR12																				BU6-2		
Mineral	Grt (Core → Rim)															Bi				Pl	Bi	Amp	Pl
																Far from Grt		Near Grt					
Spot	1	2	3	4*	5	6	7	8	9	10	11	12	13	14	15	16*	17	18	19	20*	21	22*	23*
SiO_2	38.31	38.86	38.78	38.21	36.71	38.26	38.52	38.29	38.39	38.38	38.39	37.38	38.26	38.50	38.07	35.49	35.75	35.44	35.23	60.65	37.50	45.76	53.46
TiO_2	0.05	0.02	-	0.03	0.03	-	0.00	0.03	0.01	0.04	-	0.01	0.06	0.01	-	2.37	2.50	2.48	3.34	-	1.52	0.69	0.02
Al_2O_3	20.87	21.23	21.11	21.18	20.15	21.09	21.09	21.23	20.85	21.24	21.16	20.00	21.25	21.23	21.09	18.65	18.38	18.24	17.90	23.69	16.82	10.41	27.86
FeO	28.20	27.83	28.39	28.76	27.86	28.34	28.44	28.84	28.16	28.13	27.87	27.75	27.99	28.70	28.56	15.38	15.52	16.54	16.01	0.04	11.34	11.42	0.12
MnO	4.67	4.76	4.47	4.74	4.48	4.70	4.79	4.97	5.03	5.25	5.30	5.48	5.92	5.80	6.42	0.15	0.09	0.15	0.16	-	0.06	0.23	0.01
MgO	5.94	5.95	6.01	6.09	5.68	5.85	5.94	5.86	5.87	5.69	5.48	5.04	5.37	5.11	4.74	11.66	11.65	11.48	11.08	0.02	16.47	14.20	-
CaO	1.30	1.33	1.28	1.27	1.27	1.30	1.23	1.29	1.26	1.22	1.20	1.19	1.16	1.11	1.07	-	-	-	-	6.15	0.01	12.01	11.25
Na_2O	0.09	0.03	0.03	0.05	0.16	0.03	0.03	0.04	0.08	0.07	0.03	0.18	0.04	0.01	0.01	0.24	0.21	0.27	0.19	8.99	0.12	1.39	6.00
K_2O	0.04	0.02	0.01	0.01	0.07	-	-	-	0.03	0.03	-	0.10	-	0.01	-	10.83	11.06	10.95	11.11	0.27	10.84	0.35	0.07
Total	99.46	100.01	100.09	100.33	96.39	99.57	100.04	100.54	99.68	100.04	99.42	97.12	100.06	100.48	99.96	94.79	95.14	95.54	95.01	99.80	94.69	95.73	98.80
Si	3.034	3.049	3.045	3.002	3.003	3.028	3.033	3.007	3.038	3.026	3.041	3.049	3.023	3.033	3.026	2.691	2.704	2.685	2.683	10.181	2.784	6.680	8.854
Ti	0.003	0.001	0.000	0.002	0.002	0.000	0.000	0.002	0.000	0.002	0.000	0.001	0.004	0.000	0.000	0.135	0.142	0.141	0.192	0.000	0.085	0.076	0.002
Al	1.949	1.964	1.955	1.962	1.943	1.968	1.958	1.965	1.945	1.974	1.976	1.924	1.979	1.972	1.976	1.668	1.639	1.629	1.607	4.687	1.472	1.792	5.440
Fe^{3+}	0.000	0.000	0.000	0.039	0.081	0.000	0.000	0.025	0.000	0.000	0.000	0.015	0.000	0.000	0.000	0.000	0.000	0.000	0.000	0.002	0.000	0.725	0.007
Fe^{2+}	1.868	1.826	1.865	1.851	1.825	1.876	1.874	1.870	1.863	1.854	1.847	1.878	1.849	1.891	1.899	0.975	0.982	1.048	1.020	0.003	0.704	0.669	0.010
Mn	0.313	0.316	0.297	0.315	0.310	0.315	0.320	0.331	0.337	0.351	0.356	0.379	0.396	0.387	0.432	0.010	0.006	0.010	0.010	0.000	0.004	0.028	0.002
Mg	0.701	0.696	0.704	0.714	0.692	0.690	0.697	0.686	0.692	0.668	0.647	0.613	0.632	0.600	0.562	1.318	1.313	1.297	1.257	0.005	1.822	3.089	0.000
Ca	0.111	0.112	0.108	0.107	0.111	0.110	0.103	0.108	0.107	0.103	0.102	0.104	0.098	0.094	0.091	0.000	0.000	0.000	0.000	1.106	0.001	1.879	1.996
Na	0.014	0.004	0.005	0.008	0.025	0.005	0.005	0.007	0.013	0.010	0.004	0.028	0.007	0.001	0.001	0.036	0.031	0.040	0.027	2.925	0.017	0.099	1.927
K	0.004	0.002	0.001	0.001	0.007	0.000	0.000	0.000	0.003	0.003	0.000	0.010	0.000	0.001	0.000	1.049	1.068	1.060	1.080	0.058	1.028	0.000	2.292
Fe/(Fe+Mg)	0.727	0.724	0.726	0.722	0.725	0.731	0.729	0.732	0.729	0.735	0.741	0.754	0.745	0.759	0.772	0.425	0.428	0.447	0.448				
Alm	0.624	0.619	0.627	0.620	0.621	0.627	0.626	0.624	0.621	0.623	0.626	0.631	0.622	0.636	0.636								
Spss	0.105	0.107	0.100	0.105	0.106	0.105	0.107	0.111	0.112	0.118	0.121	0.127	0.133	0.130	0.145								
Py	0.234	0.236	0.237	0.239	0.236	0.231	0.233	0.229	0.231	0.224	0.219	0.206	0.212	0.202	0.188								
Gross	0.037	0.038	0.036	0.036	0.038	0.037	0.034	0.036	0.036	0.035	0.035	0.035	0.033	0.032	0.030								
P-T conditions	698 °C, 6.4 kbar																				652 °C		

Normalized on the sum of tetrahedral and octahedral cations=6.9 and 11 oxygens for biotite. Normalized to 8 oxygens and total Fe as assumed as ferric for feldspar, to 23 oxygens and Fe^{3+} is calculated following the scheme of Dale and others (2000) for amphibole, and to 8 cations and 12 oxygens for garnet. Alm = $Fe^{2+}/(Fe^{2+}+Mg+Mn+Ca)$, Spss = $Mg/(Fe^{2+}+Mg+Mn+Ca)$, Py = $Mn/(Fe^{2+}+Mg+Mn+Ca)$, Gross = $Ca/(Fe^{2+}+Mg+Mn+Ca)$. P-T estimating for AR12 and BU6-2 were using GB-GBPQ thermobarmeter (Holdaway, 2000; Wu and others, 2004) and Amp-Pl-Qtz thermometer (Holland and Blundy, 1994), respectively.

* Analytic points (4, 16 and 20) and (22 and 23) selected for respective P-T calculation.

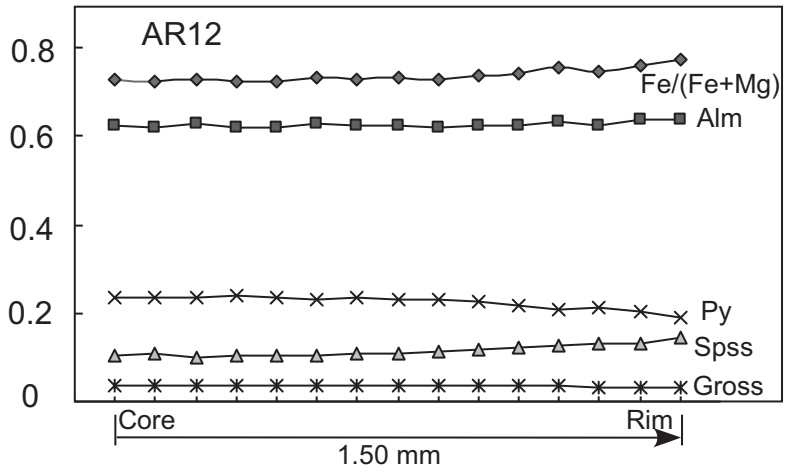

Fig. 6. Representative zoning profile of Fe/(Fe+Mg), almandine (Alm), grossular (Gross), pyrope (Py) and spessartine (Spss) from core to rim of the analyzed garnet grain from paragneiss sample AR12.

ence, 1992; Kohn and Spear, 2000). However, the effects of retrogression can be significantly minimized when garnet is not abundant, and matrix biotite is far away from the garnet grains selected (Kohn and Spear, 2000; Zhou and others, 2006). Thus, selected matrix biotite and garnet with the lowest Fe/(Fe+Mg) ratio were used to calculate the peak *P-T* conditions for sample AR12 using the GB-GBPQ Geothermobarmeter (Holdaway, 2000; Wu and others, 2004), and give results of 698 °C and 6.4 kbar.

The Ti content of zircon coexisting with rutile or other Ti-rich phases and the Zr content of rutile coexisting with zircon or other Zr-rich phase show a strong dependence on temperature, which have been recently used to construct new geothermometers (Zack and others, 2004; Watson and others, 2006; Ferry and Watson, 2007; Tomkins and others, 2007). These have a great advantage in metamorphic studies, because they can provide a direct link between the metamorphic temperature and the timing of metamorphic growth or recrystalization in the zircon. In this study, trace element compositions of zircon from paragneiss AR12 and granitic gneiss WQG4 were determined simultaneously with U-Pb isotopic compositions by LA-ICP-MS. Ti concentrations of the ~390 Ma metamorphic overgrowths were selected for temperature calculation using the thermometer developed by Ferry and Watson (2007). Because the Ti content of zircon depends on activities of SiO_2 (a_{SiO_2}) and TiO_2 (a_{TiO_2}) as well as temperature, to apply the thermometer these values must be estimated when rutile is absent. A value of silica activity equal to 1 is reasonable for these samples because abundant quartz can be observed. The absence of rutile in these samples may imply $a_{TiO_2}<1$, but the presence of ilmenite may indicate a relatively high TiO_2 activity. Values of a_{TiO_2} in most silicic melts that crystallize zircons are commonly greater than 0.5, typically 0.6 to 0.9 (Watson and others, 2006; Hayden and Watson, 2007). An intermediate value of $a_{TiO_2} = 0.75$ is assumed for the two samples. The inferred a_{TiO_2} is only weakly constrained, but deviations outside a range of a_{TiO_2} of 0.6 to 0.9 seem unlikely, as suggested in previous studies using the Ti-in-Zircon thermometer (Grimes and others, 2009; Jöns and others, 2009; Morishita and others, 2009; Simon and others, 2009). Analytical data and the calculated temperatures are presented in table 3. The Ti contents of zircon rims from sample AR12 range from 3.3 to 11.7 ppm, with an average of 6.4 ppm. The calculated temperature varies from 674 to 789 °C, with a mean value of

723 °C. The Ti contents of zircon rims from sample WQG4 range from 3.2 to 10.3 ppm, with an average of 5.9 ppm, and the estimated temperature ranges from 672 to 776 °C, with a mean value of 716 °C. Using an a_{TiO_2} of 0.6 or 0.9, instead of 0.75, changes the temperatures by +20/−16 °C and +21/−16 °C for AR12 and WQG4, respectively.

DISCUSSION

Significance of Zircon U-Pb Ages

Igneous ages.—Zircons from amphibolite sample BU6-2 occur mostly as euhedral to subhedral crystals, with oscillatory zoning and high Th/U ratios (table 1 and fig. 4A), which suggest an igneous origin. The weighted mean U-Pb age of 426 ± 3 Ma for the majority of the cores is taken to represent the crystallization age of the amphibolite protolith. The main population in granitic gneiss WQG4 is defined by analyses on the corroded zircon cores with quite similar and relatively high Th/U ratios, and high total REE, as well as some other trace element contents, including Hf, P and Y. Therefore we interpret the weighted mean U-Pb age of 463 ± 4 Ma to record the crystallization age of the precursor granite of the gneiss. The older grains in the two samples are probably xenocrysts inherited from the country rocks, because detrital zircons in the nearby metasedimentary rocks have similar age spectra with these xenocrysts, which cluster predominantly in the Early Paleozoic to Neoproterozoic and extend to the Paleoproterozoic and Archean (Long and others, 2007; Sun and others, 2008). High-grade rocks such as amphibolite BU6-2 and granitic gneiss WQG4 were previously assigned to the Precambrian (Hu and others, 2000, 2001, 2002; Wang and others, 2002). Data from this study do not support this interpretation. Furthermore, increasing evidence suggests that massive gneissic plutons in the Chinese Altai do not represent "Precambrian basement" but give mostly Paleozoic ages, for example, 460 to 375 Ma in the Central Chinese Altai and the Qiongkuer Domains (Wang and others, 2006; Sun and others, 2008, 2009) and 451 to 433 Ma in the South Chinese Altai Domain (Briggs and others, 2007). Since rocks older than 540 Ma have not been identified yet in the Chinese Altai, our new data combined with previous results lead us to question the existence of so-called Precambrian basement in the region. Zircons from paragneisses BU14 and AR12 commonly show a core-rim structure. Analyses on the rounded or fragmented cores give U-Pb ages ranging from the Early Paleozoic to Archean. Nearly 60 percent of the zircons are 450 to 590 Ma old, suggesting a significant input from Late Neoproterozoic to Early Paleozoic source rocks. These zircons have a large variation in Th, U, REE and other trace element compositions, possibly demonstrating a diverse source in the sedimentary provenance. More information on the detrital zircons was recently provided and discussed in Long and others (2007) and Sun and others (2008).

Metamorphic ages.—Studies of high-grade metamorphic rocks in the Chinese Altai have revealed a complex metamorphic history (Zhuang, 1994; Zhang and others, 2004, 2007; Wei and others, 2007). $^{40}Ar/^{39}Ar$ dating of micas and amphibole in schists and gneisses gave ages ranging from 275 to 244 Ma (Laurent-Charvet and others, 2003; Briggs and others, 2007, 2009) and monazite from greenschist/amphibolite-facies metasedimentary rocks gave *in situ* ion-microprobe Th-Pb ages of 293 to 254 Ma (Briggs and others, 2007) and chemical Th-U-total Pb isochron (CHIME) ages of 268 to 261 Ma (Zheng and others, 2007). These results clearly indicate that rocks in the Chinese Altai experienced a Late Paleozoic regional metamorphic event. This thermal event is also recorded by a mafic granulite near Fuyun city (metamorphic age of 255 Ma from Chen and others, 2006) and an orthogneiss near Qinghe city (metamorphic age of 281 Ma from Hu and others, 2006), and it is considered to be a result of a tectonic event associated with the main sinistral motion along the Erqis Fault in the Late Paleozoic (Laurent-Charvet and others, 2003). However, recent studies indicate

that the Chinese Altai may have undergone an earlier deformation/metamorphic event. For example, the deformation pattern of granitic plutons may be related to a regional event in the Early Devonian (Wang and others, 2006). A Rb-Sr whole-rock isochron age of ~365 Ma for a phyllite near Hanas was reported by Zhuang (1994) and was interpreted to represent a Middle Devonian metamorphic event (Windley and others, 2002). A metamorphic event in the Early or Middle Devonian would certainly enhance our understanding of the early evolution history in the region, but the published ages were highly speculative and no solid constraints have been provided before this study.

Due to their refractory nature, zircons are robust and may record peak metamorphic ages that are resistant to subsequent resetting (Finch and Hanchar, 2003; Kröner and others, 2004; Zheng and others, 2005; Bauer and others, 2007). In this study, zircon grains from all samples display some degree of metamorphic overgrowth or recrystallization (see fig. 3). Although the host rocks have different formation ages and detrital zircon cores from the same meta-sedimentary sample may have diverse ages, the metamorphic components give consistent $^{206}Pb/^{238}U$ ages of ~390 Ma (389 ± 6 Ma, 387± 8 Ma, 391 ± 5 Ma and 391 ± 4 Ma, for samples BU6-2, BU14, AR12 and WQG4, respectively), possibly in response to a unique metamorphic event in the Middle Paleozoic. A similar metamorphic age is also recognized in a highly deformed migmatite near Keketuohai, where Neoproterozoic–Early Paleozoic detrital zircons are surrounded by metamorphic overgrowths that give a uniform $^{206}Pb/^{238}U$ age of ~384 Ma (Long and others, 2007). Considering that the ~390 Ma metamorphic ages were obtained for samples from different locations, we suggest that a prominent Middle Paleozoic metamorphism affected a large region of the Altai orogen.

High Temperature Metamorphism in the Middle Devonian

The sillimanite zone is the most extensive metamorphic zone in the Chinese Altai, including mineral assemblages of garnet, biotite, K-feldspar, sillimanite and quartz (+muscovite, plagioclase). Rocks in this zone have been suggested as having evolved under peak *P-T* conditions of 6.3 to 6.8 kbar and 650 to 690 °C based on the KMnFMASH *P-T* calculation of one sample near Aletai city (Wei and others, 2007). In the present study, amphibolite BU6-2 records a temperature of 652 °C and garnet-sillimanite paragneiss AR12 gives *P-T* conditions of 698°C and 6.4 kbar, further confirming a relatively high-*T* condition. As discussed above, two metamorphic events have now been defined in the Chinese Altai, one in the Late Paleozoic and the other in the Middle Paleozoic. It was uncertain before this study which episode was responsible for the high-*T* metamorphism. The application of Ti-in-zircon geothermometry to zircon metamorphic components in samples AR12 and WQG4 gives temperatures of 723 °C and 716 °C respectively, which clearly indicate that these zircons were formed during the high-*T* metamorphism. Consequently, the U-Pb ages of the overgrowth and/or recrystallized zircon rims indicate that the high-*T* metamorphism occurred at ~390 Ma in the Middle Devonian.

It is noteworthy that various volcanic rocks, including magnesian andesites (adakites and boninites), high-Ti basalts and Nb-rich basalts, were erupted in the region during the Devonian (Xu and others, 2001, 2002; Zhang and others, 2003b, 2005; Niu and others, 2006a). Their original contact relationships with the high-grade rocks have been largely obliterated by subsequent strong regional deformation (Laurent-Charvet and others, 2003; Briggs and others, 2009) and now these volcanic rocks are imbricated with high-grade rocks in the southern part of Chinese Altai or occur in the tectonic mélange within the Erqis fault zone (Niu and others, 2006a; Xiao and others, 2009; Wong and others, 2010). Paleontological study of sedimentary layers interbedded with the magnesian andesites indicates a depositional age of Middle Devonian (Niu and others, 2006a). Zircon grains from the felsic member of bimodal volcanic

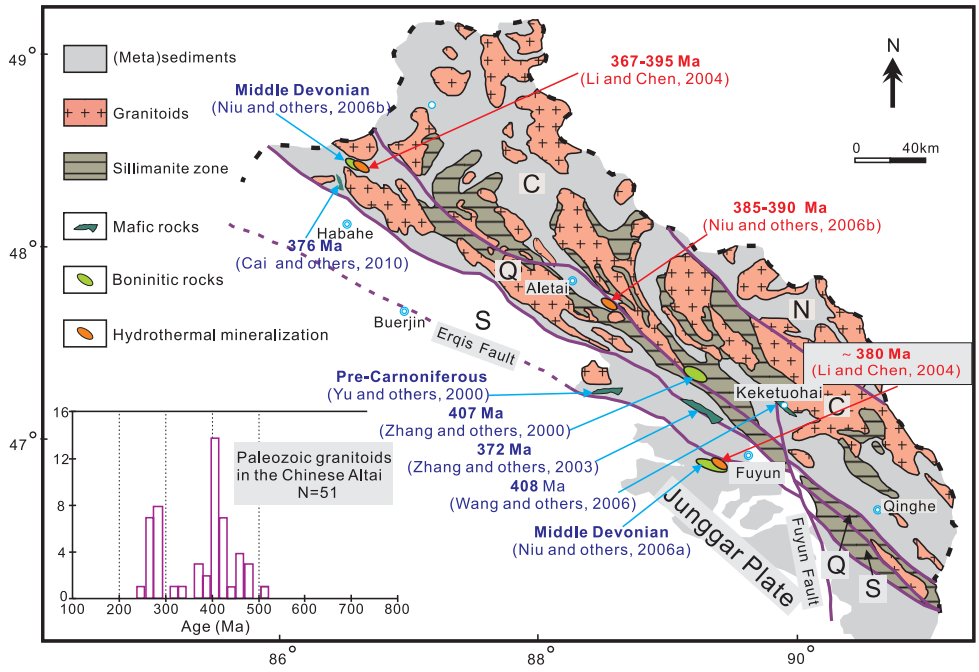

Fig. 7. Simplified geological map of the Chinese Altai showing the rock types, hydrothermal mineralization and domains. The inset age histogram for Paleozoic granitoids in the Chinese Altai shows a clear decline in the volume of typical arc-magmatism in the time interval of 410–370 Ma. Data sources for Paleozoic granitoids in the Chinese Altai are from Wang and others (2006), Tong and others (2007), Yuan and others (2007), Sun and others (2008). Domain symbols as in figure 1.

rocks near sample AR12 were dated at 407 Ma (Zhang and others, 2000). The Kuerti mafic rocks, 40 km northwest of Fuyun city, were considered to have erupted during seafloor spreading in a back arc basin (Xu and others, 2002), and SHRIMP U-Pb zircon analyses of associated plagiogranite gave an age of 372 ± 19 Ma (Zhang and others, 2003a). Some mafic dikes, possibly the intrusive counterparts of these volcanic rocks, sporadically distributed in and around the high-*T* sillimanite zone, also have broadly similar Middle Devonian ages (see fig. 7). For example, mafic intrusions near Habahe and Keketuohai gave zircon U-Pb ages of 376 ± 5 Ma (Cai and others, 2010) and 408 ± 6 Ma (Wang and others, 2006), respectively. Geochemically, these rocks are characterized by low total REE and U-shaped patterns, suggesting magma generation from a strongly depleted source (Xu and others, 2001, 2002; Niu and others, 2006a; Cai and others, 2010; Wong and others, 2010). All available $\varepsilon_{Nd}(t)$ data from these rocks give quite high positive values (+7 to +9, see Xu and others, 2001, 2002; Zhang and others, 2003b; Niu and others, 2006a; Cai and others, 2010). Igneous zircons from doleritic dikes near Habahe all show positive $\varepsilon_{Hf}(t)$ values from +10.7 to +13.8 (Cai and others, 2010). The tectonic environment accounting for the generation of these diagnostic rocks has been the subject of much controversy, which will be discussed in more detail in the next section. Nevertheless, there seems a consensus that these rocks were formed due to the upwelling of hot asthenospheric mantle in the region (Niu and others, 2006a; Cai and others 2010; Wong and others, 2010), similar to that reported by Macpherson and Hall (2001) for Eocene boninite in the Izu-Bonin-Mariana arc. The strong coincidence of the diversified volcanic/intrusive rocks and high-*T* metamor-

phism at ~390 Ma apparently indicates some genetic link and may imply a high geothermal gradient in the region.

Mechanism for the High-T Metamorphism

Previous interpretation.—High-*T*/low-*P* metamorphic terranes commonly preserve apparently anomalous thermal conditions and permit unique insights into the regional thermal-tectonic evolution of an area. Recent studies indicate that high-*T*/low-*P* metamorphism could be attributed to arc magmatism (Dymoke and Sandiford, 1992; Graeßner and Schenk, 1999; Pitra and Waal, 2001), crustal extension (Bodorkos and others, 2002), crustal thickening (White, 2005) or ridge-trench interaction (Azpiroz and others, 2006). Irrespective of their tectonic environment, the generation of high-*T*/low-*P* metamorphic rocks generally requires a large heat input and is commonly related to an anomalously high conductive heat flow rather than steady-state conductive thermal regimes in the lower crust (Sisson and others, 1989). In the Chinese Altai, the high-*T*/low-*P* metamorphic sequence (andalusite-sillimanite-cordierite) constructs a relatively high geothermal gradient of 28 to 52 °C/km, which is significantly different from that of the medium-*P* (kyanite-type) sequence (21-26 °C/km) in the region (Zhang and others, 2007; Wei and others, 2007). The ~720 °C temperature estimated by Ti-in-zircon thermometry may have resulted in considerable partial melting (see Spear and others, 1999; White and others, 2001). This inference is evidenced by the extensive occurrence of migmatized rocks in the Chinese Altai (see Long and others, 2007; Wei and others, 2007; Sun and others, 2008). Such a high temperature signature generally implies uncommonly elevated heat flux from a deep-seated source (De Yoreo and others, 1991). To account for the increased heat, rifting (He and others, 1990) or emplacement of granitic intrusions (Zhuang, 1994; Zhang and others, 2007) have been previously invoked as possible causes. However, the hypothesis of rifting is highly speculative and the tectonic evidence for rifting at ~390 Ma has never been presented or discussed. The high-*T* metamorphism was regional, rather than contact. Even if the development of high-*T* metamorphism is coeval with the emplacement of some granites, it should not be simply treated as the consequence of their intrusion, because the granitic intrusions themselves also were possibly generated from the elevated heat flux which resulted in the high-*T* metamorphism.

On the basis of the geochemical signatures of the Devonian magnesian andesites, high-Ti and Nb-rich basalts and various mafic intrusions, researchers have envisaged models of back-arc spreading (Xu and others, 2002; Wang and others, 2006) or slab break-off (Niu and others, 2006a) to interpret the upwelling of the hot asthenospheric materials, which could contribute to the high geothermal gradient in the region. For example, the ~375 Ma Kuerti mafic rocks were considered to have erupted during seafloor spreading in a back-arc basin (Xu and others, 2002). This mafic complex and its associated radiolarian chert were interpreted by Wang and others (2006) as ophiolitic fragments marking the sites of back-arc basin closure. We note that extensive back-arc spreading, as in the present west Pacific (Hawkins and others, 1990) and south Pacific (Gribble and others, 1998), generally occurs where subducted lithosphere is relatively old (>80 Ma) and thereby cold and dense. In contrast, the occurrence of adakite and boninite in the region suggest a comparatively young and buoyant subduction system. A slab break-off model was once proposed for the Altai to explain the close association of boninite in ophiolite, in which Devonian boninitic rocks were suggested to be generated in the fore-arc region due to the upwelling of hot asthenosphere (Niu and others, 2006a). However, slab break-off has generally been suggested to take place during continental collisions which are preceded by subduction of dense oceanic lithosphere and followed by attempted subduction of buoyant continental lithosphere (Davies and von Blanckenburg, 1995; Teng and others, 2000).

However, it appears that there is no clear evidence to support a Devonian continental collision in the Chinese Altai. In summary, the previously proposed tectonic models are not supported by the geological observations, and thus cannot adequately account for the ~390 Ma high-*T* metamorphism.

Ridge subduction and high-T metamorphism.—Interaction of sea-floor-spreading ridges with subduction systems has been a topic of interest in recent years. Due to the unique physical and thermal structure of oceanic ridges, ridge subduction would have a pronounced influence on the thermal structure of the subduction system, as well as the nature of the magmatism (Sisson and Pavlis, 1993; Nakajima, 1994; Kinoshita, 1995; Thorkelson, 1996; Brown, 1998). It is generally accepted that the consumption of an ocean basin by subduction commonly brings a sea-floor-spreading ridge toward a deep-sea trench. As a result, the oceanic slabs on both sides will progressively unzip during the descent of the spreading ridge, followed by the formation of a gap called a "slab window" (Dickinson and Snyder, 1979; Thorkelson, 1996). The opening of the slab window will give rise to ascending mantle materials which will lead to melting of the down-going slab and significant metasomatism of the mantle wedge (Schiano and others, 1995; Prouteau and others, 2001). The uplift of hot asthenosphere will then lead to an increase in the geothermal gradient of the overriding plate and trigger crustal anatexis and high temperature metamorphism (Sisson and Pavlis, 1993; Lagabrielle and others, 2000; Sisson and others, 2003a). This geological phenomenon has been well documented in constructing the crustal growth along the circum-pacific belt in Japan, Ecuador, the Aleutians and Baja California (Sisson and others, 2003a; Chadwick and others, 2009; Cole and Stewart, 2009). Although the development of high-*T* metamorphism is not unique to ridge subduction, when combined with the diverse composition of igneous rocks, for example, magnesian andesites, adakites, and a variety of mafic dikes, it may be a diagnostic signature for ridge-subduction (Iwamori, 2000; Sisson and others, 2003a, 2003b; Santosh and Kusky, 2010).

Middle Devonian ridge subduction in the Chinese Altai.—Ridge subduction was recently postulated as a dominant tectonic control in the geodynamic evolution of the CAOB by Windley and others (2007). They considered that the subduction of a spreading ridge provided abundant heat and juvenile materials to induce massive magmatism, as documented in Jahn and others (2000), where voluminous granitic intrusions have low initial Sr isotopic ratios and positive $\varepsilon_{Nd}(t)$ values. They also suggested that the high-*T* metamorphism, chemically distinctive rocks (for example, adakites and boninites) and extensive hydrothermal mineralization in the CAOB were common for ridge subduction. They argued that repeated ridge-trench interaction may have occurred over a long time period between 1000 and 250 Ma in the CAOB, which is supported by recent case studies (for example, Jian and others, 2008; Geng and others, 2009; Liu and others, 2009; Sun and others, 2009; Tang and others, 2010). The development of high-*T* metamorphism coincidences with the occurrence of various volcanic rocks and diverse mafic intrusions around 390 Ma in the Chinese Altai and all of these features can be accommodated by the ridge subduction model.

Recent zircon U-Pb isotopic studies on granitoid rocks from the Chinese Altai indicate that magmatic activity occurred intermittently from 520 to 370 Ma (Windley and others, 2002; Wang and others, 2006; Yuan and others, 2007; Sun and others, 2008), with a dominant peak at 400 Ma (Tong and others, 2007). The geochemical data of all these rocks show subduction signatures. Hf isotopic compositions for zircons of igneous origin show a dramatic change at 410 Ma. Before this time, $\varepsilon_{Hf}(t)$ values were either positive or negative (−18 to +15), but after this time they all became positive (0 to +16), indicating that the contribution of juvenile material in the magma source became dominant after ~410 Ma (Sun and others, 2009). The abrupt change in Hf isotopic compositions may imply a dramatic change in the composition of the

lithosphere, as zircon mostly crystallizes in intermediate-silicic magmas that originate in the lithosphere. The ridge subduction model can readily accommodate this process, as the formation of a slab window will produce anomalous conditions of thermal, physical and chemical state in the surrounding mantle. As a consequence, the upwelling of asthenospheric materials, in turn, will affect the tectonic and magmatic evolution of the overriding plate (Thorkelson, 1996). This model can also explain the magmatic pattern in the Chinese Altai, in which the amount of typical island arc rocks dramatically decreased from ~410 Ma to ~370 Ma (Cai and others, 2008), whereas magnesian andesites and mafic intrusions first appear in this period (see fig. 7). The transition from typical island arc rocks to magnesian andesites and mafic intrusions may result from possible ridge-trench interaction (Brown, 1998).

The ridge subduction model can also provide a feasible interpretation for the extensive hydrothermal mineralization in the region (see fig. 7). Polymetallic deposits occur in association with Devonian sedimentary rocks in the southern Altai and commonly have mineralization ages similar to that of the high-*T* regional metamorphism. For example, fluid inclusions within quartz from the Ashele sulfide deposit (15 km north of Habahe) and the Sarekuobu gold deposit near Fuyun city gave Rb-Sr isochron ages of 367 and 395 Ma, respectively (Li and Chen, 2004), which were taken to represent the mineralization age. Ore minerals (pyrite, magnetite and galena) in the Abagong iron deposit (25 km southeast of Aletai city) gave Pb model ages of 385 to 390 Ma (Niu and others, 2006b). Sulfur and O isotopic studies of magnetite from the Abagong iron deposit indicate that the ore-forming fluids had $\delta^{34}S$ of −4.3 permil to −1 permil (avg. −1.6‰) and $\delta^{18}O$ higher than 7 permil, both implying a deep-seated origin (Niu and others, 2006b). Other lines of evidence include the recent Pb isotopic data for some of these ore deposits, which have consistently low $^{207}Pb/^{204}Pb$ values, suggesting a dominant mantle contribution (Chiaradia and others, 2006). The strong coincidence between the hydrothermal mineralization and high-*T* metamorphism is probably due to the elevated heat flux with uncommonly large fluxes of aqueous fluids (De Yoreo and others, 1991), again a common feature for ridge subduction (Windley and others, 2007).

Taken together, the notable geological features, especially the high-*T* metamorphism in the Middle Paleozoic in the Chinese Altai, can be best explained by the subduction of an active oceanic spreading ridge. A simplified scenario of subduction of an oceanic spreading ridge in the region can be depicted as follows (fig. 8): (1) an active continental margin developed in the Early Paleozoic due to the progressive subduction of Paleo-Asian oceanic crust (Windley and others, 2002; Sun and others, 2008). This process produced a large amount of magmatic rocks, as manifested by significant magmatic activities between 520 and 410 Ma in the region (Windley and others, 2002; Wang and others, 2006; Yuan and others, 2007; Sun and others, 2008). (2) an active spreading ridge approached and descended underneath the trench around 410 Ma, resulting in the formation of a slab window. Upwelling of the asthenosphere caused thermal erosion of the window margins and metasomatism of the mantle wedge that generated chemically distinctive rocks, including magnesian andesites, adakites, boninites and diverse mafic dikes (Xu and others, 2001, 2002; Zhang and others, 2003b, 2005; Niu and others, 2006a; Cai and others, 2010; Wong and others, 2010). The overriding lithosphere was then significantly changed in its physical and chemical characteristics, as suggested by the abrupt change in zircon $\varepsilon_{Hf}(t)$ values around 410 Ma (Sun and others, 2009) and a decline in the volume of typical calc-alkaline arc magmatism, accompanied by an increase in high-Mg andesite and tholeiitic mafic magmatism in the time interval of 410 to 370 Ma (Xu and others, 2002; Niu and others, 2006a; Cai and others, 2010). Ascending hot mantle materials would also create anomalously elevated thermal gradients and have the capacity to

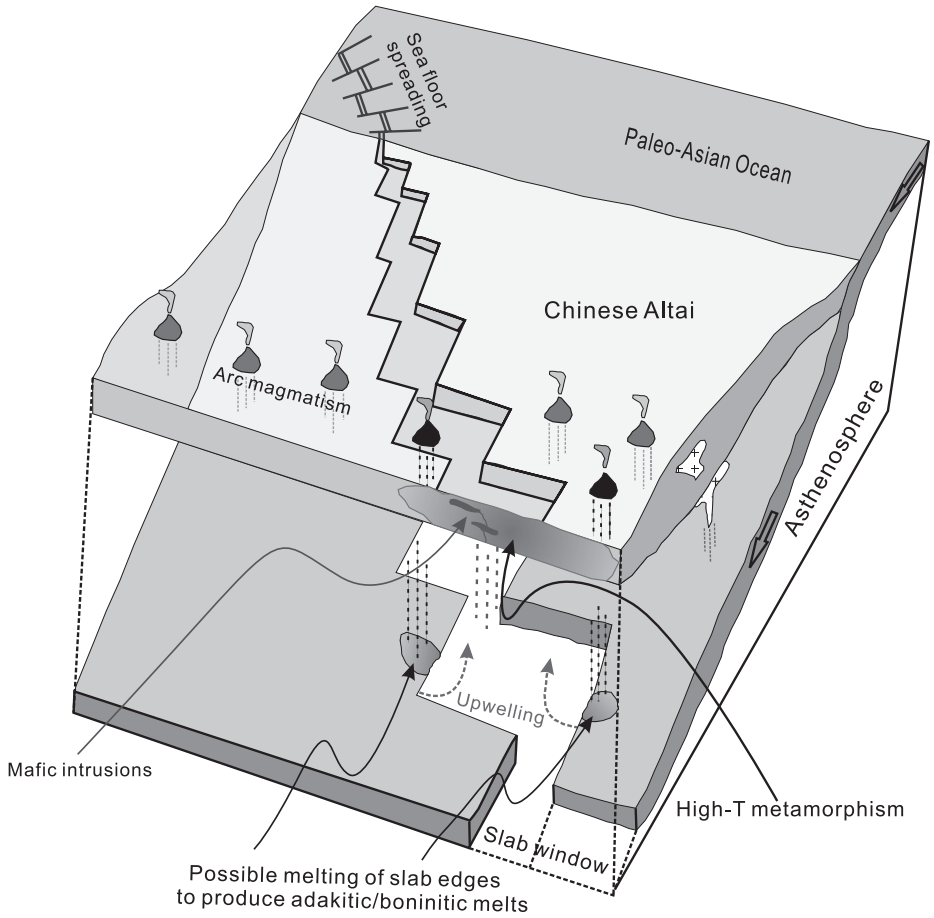

Fig. 8. Ridge subduction and slab window model proposed in this study for the origin of the high-*T* metamorphism (modified after Thorkelson, 1996; Santosh and Kusky, 2010). When the spreading ridge becomes progressively immersed in hot asthenosphere, the slab on either side continues to diverge but ceases to grow, resulting in an ever-widening gap between two subducting oceanic slabs called a slab window. The upwelling of asthenospheric mantle would alter the style of magmatism on the overriding plate, as well as triggering high-*T* metamorphism.

contribute significantly to the thermal budgets of the high-*T*/low-*P* metamorphism in the overriding plate. The ~390 Ma high-*T* metamorphism event investigated in this study could be a direct consequence of Devonian ridge subduction in the region.

Tectonic Significance

Ocean floor forms at spreading ridges and is largely consumed in subduction zones (Thorkelson, 1996). The spreading ridge is ultimately brought to a deep-sea trench by the successive down-going of the oceanic slab (Thorkelson, 1996; Brown, 1998; Windley and others, 2007). This means that arc magmatism, a normal consequence of subduction, must occur prior to the subduction system interacting with the spreading ridge. In this study, the high-*T* metamorphism and magmatism in the Middle Paleozoic are considered to be the result of ridge subduction. We thus favor the recently proposed tectonic scenario that the Altai could be an active continental margin in the Early-Middle Paleozoic (Windley and others, 2002; Xiao and others,

2004; Wang and others, 2006; Long and others, 2007, 2008; Sun and others, 2008), rather than a passive one (He and others, 1990; Li and others, 2006).

Regional metamorphism in the Chinese Altai was previously thought to have occurred as one event, and both low- and high-grade metamorphism were considered to have developed during the Permian. However, a prominent ~390 Ma high-*T* metamorphic event is confirmed by this study. Therefore, the Chinese Altai experienced multiple metamorphic events in the Paleozoic. Rocks from the biotite, garnet and staurolite zones preserve a typical burial and exhumation history possibly in the Late Paleozoic (Wei and others, 2007). Rocks in the higher grade portion, however, recorded a high-temperature regime in the Middle Paleozoic, which may be related to ridge subduction. Therefore, our present work suggests that the metamorphic rocks in the Chinese Altai cannot be simply regarded as only the response to Late Paleozoic tectonic events in the region, and the prolonged thermal-tectonic processes from the Middle Devonian to Permian require further detailed investigation.

The tectonic evolution of the CAOB has been explained by several competing models: for example, (i) punctuated accretion by closure of multiple oceans (Coleman, 1989), (ii) closure and accretion of new oceans, arcs and micro-continents (Mossakovsky and others, 1993), (iii) continuous forearc accretion of a single subduction zone (Sengör and others, 1993; Sengör and Natal'in, 1996), and (iv) fore-arc accretion punctuated by back-arc opening and closure (Yakubchuk and others, 2002). More recently, the evolution of this belt has been interpreted in the light of the modern western Pacific tectonics (Mossakovsky and others, 1993; Badarch and others, 2002; Khain and others, 2003; Buslov and others, 2004; Windley and others, 2007; Xiao and others, 2009). These authors suggested that the geology of the CAOB is characteristic of a paleo-archipelago, and that the *ca.* 800 Ma prolonged development can be best understood in terms of multiple accretionary processes, similar to that in Indonesia (Hall and Spakman, 2002). Data from the Chinese Altai (for example, Sun and others, 2009; Wong and others, 2010 and this work) together with the case studies of 451 to 434 Ma and 315 to 305 Ma ridge-subduction processes in Inner Mongolia (Jian and others, 2008) and West Junggar (Geng and others, 2009; Liu and others, 2009; Tang and others, 2010), indicate that multiple subduction systems were involved in the closure of the Paleo-Asian Ocean and thus favor the multiple subduction-accretion model (for example, Windley and others, 2007; Xiao and others, 2009).

CONCLUSIONS

The U-Pb isotopic analysis of metamorphic overgrowths and recrystallized domains of zircons from high-grade rocks in the Chinese Altai indicates a prominent metamorphic event at ~390 Ma in the region. Temperature estimations for the whole rocks and for the metamorphic zircon rims both give relatively high temperatures up to ~720 °C for the metamorphism. Combined with other regional geological features, our results suggest that the development of this high-*T* metamorphism probably involved subduction of an active oceanic spreading ridge in the Devonian.

ACKNOWLEDGMENTS

This study was supported by research grants from the National Basic Research Program of China (2007CB411308), Hong Kong Research Grants Council (HKU7043/07P), HKU research grants, Hong Kong-Germany Joint Research Scheme, and CAS/SAFEA International Partnership Program for Creative Research Teams. Xie Liewen and Yang Yueheng are thanked for laboratory assistance. We wish to also thank Kenny Wong, Geng Hongyan and Cai Keda for their great help during our field investigation. This study was inspired by Professor Alfred Kröner, and the authors are grateful for his continuous scientific encouragement and guidance. Dick Glen, Lifei Zhang and

Simon Wilde (guest editor) are thanked for their comments and suggestions which significantly improved the manuscript.

References

Andersen, T., 2002, Correction of common lead in U-Pb analyses that do not report ^{204}Pb: Chemical Geology, n. 1–2, v. 192, p. 59–79, doi:10.1016/S0009-2541(02)00195-X.

Azpiroz, M. D., Fernández, C., Castro, A., and El-Biad, M., 2006, Tectonometamorphic evolution of the Aracena metamorphic belt (SW Spain) resulting from ridge-trench interaction during Variscan plate convergence: Tectonics, v. 25, TC1001, 20 p., doi:10.1029/2004TC001742.

Badarch, G., Cunningham, W. D., and Windley, B. F., 2002, A new terrane subdivision for Mongolia: implications for the Phanerozoic crustal growth of Central Asia: Journal of Asian Earth Sciences, v. 21, n. 1, p. 87–110, doi:10.1016/S1367-9120(02)00017-2.

Bauer, C., Rubatto, D., Krenn, K., Proyer, A., and Hoinkes, G., 2007, A zircon study from the Rhodope metamorphic complex, N-Greece: Time record of a multistage evolution: Lithos, v. 99, n. 3–4, p. 207–228, doi:10.1016/j.lithos.2007.05.003.

Belousova, E. A, Griffin, W. L, O'Reilly, S. Y., and Fisher, N. I., 2002, Igneous zircon: trace element composition as an indicator of source rock type: Contributions to Mineralogy and Petrology, v. 143, n. 5, p. 602–622, doi:10.1007/s00410-002-0364-7.

Bodorkos, S., Sandiford, M., Oliver, N. H. S., and Cawood, P. A., 2002, High-*T*, low-*P* metamorphism in the Palaeoproterozoic Halls Creek Orogen, northern Australia: the middle crustal response to a mantle-related transient thermal pulse: Journal of Metamorphic Geology, v. 20, n. 2, p. 217–237, doi:10.1046/j.1525-1314.2002.00339.x.

Briggs, S. M., Yin, A., Manning, C. E., Chen, Z.-L., Wang, X.-F., and Grove, M., 2007, Late Paleozoic tectonic history of the Ertix fault in the Chinese Altai and its implications for the development of the Central Asian Orogenic System: Geological Society of America Bulletin, v. 119, n. 7–8, p. 944–960, doi:10.1130/B26044.1.

Briggs, S. M., Yin, A., Manning, C. E., Chen, Z.-L. and Wang, X.-F., 2009, Tectonic development of the southern Chinese Altai Range as determined by structural geology, thermobarometry, ^{40}Ar/^{39}Ar thermochronology, and Th/Pb ion-microprobe monazite geochronology: Geological Society of America Bulletin, v. 121, p. 1381–1393, doi:10.1130/B26385.1.

Brown, M., 1998, Ridge-trench interactions and high-*T*-low-*P* metamorphism, with particular reference to the Cretaceous evolution of the Japanese Islands: Geological Society, London, Special Publications, v. 138, p. 137–169, doi:10.1144/GSL.SP.1996.138.01.09.

Buslov, M. M., Fujiwara, Y., Iwata, K., and Semakov, N. N., 2004, Late Paleozoic–Early Mesozoic Geodynamics of Central Asia: Gondwana Research, v. 7, n. 3, p. 791–808, doi:10.1016/S1342-937X(05)71064-9.

Cai, K. D., Sun, M., Yuan, C., Zhao, G. C., Xiao, W. J., Long, X. P., and Wu, F. Y., 2008, Zircon U-Pb and Hf isotopic study of granitoids from the Chinese Altai: Constraints on the Paleozoic tectonics and crustal evolution: Gondwana 13, Abstract with Programs, p. 17.

Cai, K., Sun, M., Yuan, C., Zhao, G., Xiao, W., Long, X., and Wu, F., 2010, Geochronological and geochemical study of mafic dykes from the northwest Chinese Altai: Implications for petrogenesis and tectonic evolution: Gondwana Research, v. 18, n. 4, p. 638–652, doi:10.1016/j.gr.2010.02.010.

Chadwick, J., Perfit, M., McInnes, B., Kamenov, G., Plank, T., Jonasson, I., and Chadwick, C., 2009, Arc lavas on both sides of a trench: Slab window effects at the Solomon Islands triple junction, SW Pacific: Earth and Planetary Science Letters, v. 279, n. 3–4, p. 293–302, doi:10.1016/j.epsl.2009.01.001.

Chen, H. L., Yang, S. F., Li, Z. L., Yu, X., Xiao, W. J., Yuan, C., Lin, X. B., and Li, J. L, 2006, Zircon SHRIMP U-Pb chronology of Fuyun basic granulite and its tectonic significance in Altaid orogenic belt: Acta Petrologica Sinica, v. 22, p. 1351–1358 (in Chinese with English abstract).

Chiaradia, M., Konopelko, D., Seltmann, R., and Cliff, R. A., 2006, Lead isotope variations across terrane boundaries of the Tien Shan and Chinese Altay: Mineralium Deposita, v. 41, n. 5, p. 411–428, doi:10.1007/s00126-006-0070-x.

Cole, R. B., and Stewart, B. W., 2009, Continental margin volcanism at sites of spreading ridge subduction: Examples from southern Alaska and western California: Tectonophysics, v. 464, n. 1–4, p. 118–136, doi:10.1016/j.tecto.2007.12.005.

Coleman, R., 1989, Continental growth of Northwest China: Tectonics, v. 8, n. 3, p. 621–635, doi:10.1029/TC008i003p00621.

Corfu, F., Hanchar, J. M., Hoskin, P. W. O., and Kinny, P., 2003, Atlas of Zircon Textures: Reviews in Mineralogy and Geochemistry, v. 53, n. 1, p. 469–500, doi:10.2113/0530469.

Dale, J., Holland, T., and Powell, R., 2000, Hornblende-garnet-plagioclase thermobarometry: a natural assemblage calibration of the thermodynamics of hornblende: Contributions to Mineralogy and Petrology, v. 140, p. 353–362, doi:10.1007/s004100000187.

Davies, J. H., and von Blanckenburg, F., 1995, Slab breakoff: A model of lithosphere detachment and its test in the magmatism and deformation of collisional orogens: Earth and Planetary Science Letters, v. 129, n. 1–4, p. 85–102, doi:10.1016/0012-821X(94)00237-S.

De Yoreo, J. J., Lux, D. R., and Guidotti, C. V., 1991, Thermal modeling in low-pressure/high-temperature metamorphic belts: Tectonophysics, v. 188, n. 3–4, p. 209–238, doi:10.1016/0040-1951(91)90457-4.

Dickinson, W. R., and Snyder, W. S., 1979, Geometry of subducted slabs related to San-Andreas transform: Journal of Geology, v. 87, p. 609–627, doi:10.1086/628456.

Didenko, A. N., Mossakovsky, A. A., Pechersky, D. M., Ruzhentsev, S. V., Samygin, S. G., and Kheraskova, T. N., 1994, Geodynamics of the Paleozoic oceans of the Central Asia: Russian Geology and Geophysics, v. 7–8, p. 59–76.

Dymoke, P., and Sandiford, M., 1992, Phase relationships in Buchan facies series pelitic assemblages: calculations with application to andalusite-staurolite parageneses in the Mount Lofty Ranges, South Australia: Contributions to Mineralogy and Petrology, v. 110, n. 1, p. 121–132, doi:10.1007/BF00310886.

Ferry, J. M., and Watson, E. B., 2007, New thermodynamic models and revised calibrations for the Ti-in-zircon and Zr-in-rutile thermometers: Contributions to Mineralogy and Petrology, v. 154, n. 4, p. 429–437, doi:10.1007/s00410-007-0201-0.

Finch, R. J., and Hanchar, J. M., 2003, Structure and chemistry of zircon and zircon-group minerals: Reviews in Mineralogy and Geochemistry, v. 53, n. 1, p. 1–21, doi:10.2113/0530001.

Gao, T., Chen, J., Xie, Z., Yang, S., and Yu, G., 2004, Zircon SHRIMP U-Pb age of garnet olivine pyroxenite at Hujialin in the Sulu terrane and its geological significance: Chinese Science Bulletin, v. 49, p. 2198–2204, doi:10.1007/BF03185788.

Geng, H., Sun, M., Yuan, C., Xiao, W., Xian, W., Zhao, G., Zhang, L., Wong, K., and Wu, F., 2009, Geochemical, Sr-Nd and zircon U-Pb-Hf isotopic studies of Late Carboniferous magmatism in the West Junggar, Xinjiang: implications for ridge subduction?: Chemical Geology, v. 266, n. 3–4, p. 364–389, doi:10.1016/j.chemgeo.2009.07.001.

Graeßner, T., and Schenk, V., 1999, Low-pressure metamorphism of Palaeozoic pelites in the Aspromonte, southern Calabria: constraints for the thermal evolution in the Calabrian crustal cross-section during the Hercynian orogeny: Journal of Metamorphic Geology, v. 17, p. 157–172, doi:10.1046/j.1525-1314.1999.00188.x.

Gribble, R. F., Stern, R. J., Newman, S., Bloomer, S. H., and O'Hearn, T., 1998, Chemical and Isotopic Composition of Lavas from the Northern Mariana Trough: Implications for Magmagenesis in Back-arc Basins: Journal of Petrology, v. 39, n. 1, p. 125–154, doi:10.1093/petroj/39.1.125.

Grimes, C. B., John, B. E., Cheadle, M. J., Mazdab, F. K., Wooden, J. L., Swapp, S., and Schwartz, J. J., 2009, On the occurrence, trace element geochemistry, and crystallization history of zircon from in situ ocean lithosphere: Contributions to Mineralogy and Petrology, v. 158, n. 6, p. 757–783, doi:10.1007/s00410-009-0409-2.

Hall, R., and Spakman, W., 2002, Subducted slabs beneath the eastern Indonesia-Tonga region: insights from tomography: Earth and Planetary Science Letters, v. 201, n. 2, p. 321–336, doi:10.1016/S0012-821X(02)00705-7.

Hanchar, J. M., and Rudnick, R. L., 1995, Revealing hidden structures: The application of Cathodoluminescense and back-scattered electron imaging to dating zircons from lower crustal xenoliths: Lithos, v. 36, n. 3–4, p. 289–303, doi:10.1016/0024-4937(95)00022-4.

Hawkins, J. W., Lonsdale, P. F., Macdougall, J. D., and Volpe, A. M., 1990,. Petrology of the axial ridge of the Mariana Trough backarc spreading center: Earth and Planetary Science Letters, v. 100, n. 1–3, p. 226–250, doi:10.1016/0012-821X(90)90187-3.

Hayden, L. A., and Watson, E. B., 2007, Rutile saturation in hydrous siliceous melts and its bearing on Ti-thermometry of quartz and zircon: Earth and Planetary Science Letters, v. 258, n. 3–4, p. 561–568, doi:10.1016/j.epsl.2007.04.020.

He, G. Q., Han, B. F., Yue, Y. J., and Wang, J. H., 1990, Tectonic division and crustal evolution of Altai Orogenic Belt in China: Xinjiang Geology, v. 2, p. 9–20 (in Chinese with English abstract).

Holdaway, M. J., 2000, Application of new experimental and garnet Margules data to the garnet-biotite geothermometer: American Mineralogist, v. 85, p. 881–892.

Holland, T., and Blundy, J., 1994, Non-ideal interactions in calcic amphiboles and their bearing on amphibole-plagioclase thermometry: Contributions to Mineralogy and Petrology, v. 116, n. 4, p. 433–447, doi:10.1007/BF00310910.

Hoskin, P. W. O., and Black, L. P., 2000, Metamorphic zircon formation by solid-state recrystallization of protolith igneous zircon: Journal of Metamorphic Geology, v. 18, n. 4, p. 423–439, doi:10.1046/j.1525-1314.2000.00266.x.

Hoskin, P. W. O., and Schaltegger, U., 2003, The composition of zircon and igneous and metamorphic petrogenesis: Reviews in Mineralogy and Geochemistry, v. 53, n. 1, p. 27–62, doi:10.2113/0530027.

Hu, A., Jahn, B., Zhang, G., Chen, Y., and Zhang, Q., 2000, Crustal evolution and Phanerozoic crustal growth in northern Xinjiang: Nd isotopic evidence. Part I. Isotopic characterization of basement rocks: Tectonophysics, v. 328, n. 1–2, p. 15–51, doi:10.1016/S0040-1951(00)00176-1.

Hu, A. Q., Wei, G. J., Deng, W. F., and Chen, L. L., 2006, SHRIMP zircon U-Pb dating and its significance for gneisses from the southern west area to Qinghe County in the Altai, China: Acta Petrologica Sinica, v. 22, n. 1, p. 1–10 (in Chinese with English abstract).

Hu, Z. Q., Zhang, G. X., Chen, Y. B., and Zhang, Q. F., 2001, A model of division of the continental crust basement and the time scales of the major geological events in the Xinjiang: based on studies of isotopic geochronology and geochemistry: Xinjiang Geology, v. 19, p. 12–19 (in Chinese).

Hu, Z. Q., Zhang, G. X., Zhang, Q. F., Li, T. D., and Zhang, J. B., 2002, A review on ages of Precambrian metamorphic rocks from Altai orogen in Xinjiang, NW China: Chinese Journal of Geology, v. 37, p. 129–142 (in Chinese).

Huang, X., Xu, Y., Liu, D., and Jian, P., 2003, Paleoproterozoic lower crust beneath Nushan in Anhui Province: Evidence from zircon SHRIMP U-Pb dating on granulite xenoliths in Cenozoic alkali basalt: Chinese Science Bulletin, v. 48, n. 13, p. 1381–1385.

Iwamori, H., 2000, Thermal effects of ridge subduction and its implications for the origin of granitic batholiths and paired metamorphic belts: Earth and Planetary Science Letters, v. 181, n. 1–2, p. 131–144, doi:10.1016/S0012-821X(00)00182-5.

Jahn, B. M., 2004, The Central Asian Orogenic Belt and growth of the continental crust in the Phanerozoic, *in* Malpas, J., Fletcher, C. J. N., Ali, J. R., and Aitchison, J. C., editors, Aspects of the Tectonic Evolution of China: Geological Society, London, Special Publications, v. 226, p. 73–100, doi:10.1144/GSL.SP.2004.226.01.05.

Jahn, B. M., Wu, F. Y., and Chen, B., 2000, Massive granitoid generation in Central Asia: Nd isotope evidence and implication for continental growth in the Phanerozoic: Episodes, v. 23, p. 82–92.

Jian, P., Liu, D., Kröner, A., Windley, B. F., Shi, Y., Zhang, F., Shi, G., Miao, L., Zhang, W., Zhang, Q., Zhang, L., and Ren, J., 2008, Time scale of an early to mid-Paleozoic orogenic cycle of the long-lived Central Asian Orogenic Belt, Inner Mongolia of China: Implications for continental growth: Lithos, v. 101, n. 3–4, p. 233–259, doi:10.1016/j.lithos.2007.07.005.

Jöns, N., Bach, W., and Schroeder, T., 2009, Formation and alteration of plagiogranites in an ultramafic-hosted detachment fault at the Mid-Atlantic Ridge (ODP Leg 209): Contributions to Mineralogy and Petrology, v. 157, p. 625–639, doi:10.1007/s00410-008-0357-2.

Kane, J. S., 1998, A history of the development and the certification of NIST glass SRMs 610–617: Geostandards Newsletter: The Journal of Geostandards and Geoanalysis, v. 22, n. 1, p. 7–13, doi:10.1111/j.1751-908X.1998.tb00541.x.

Khain, E. V., Bibikova, E. V., Kröner, A., Zhuravlev, D. Z., Sklyarov, E. V., Fedotova, A. A., and Kravchenko-Berezhnoy, I. R, 2002, The most ancient ophiolite of the Central Asian fold belt: U-Pb and Pb-Pb zircon ages for the Dunzhugur Complex, Eastern Sayan, Siberia, and geodynamic implications: Earth and Planetary Science Letters, v. 199, n. 3–4, p. 311–325, doi:10.1016/S0012-821X(02)00587-3.

Khain, E. V., Bibikova, E. V., Salnikova, E. B., Kröner, A., Gibsher, A. S., Didenko, A. N., Degtyarev, K. E., and Fedotova, A. A, 2003, The Palaeo-Asian Ocean in the Neoproterozoic and early Palaeozoic: new geochronologic data and palaeotectonic reconstructions: Precambrian Research, v. 122, n. 1–4, p. 329–358, doi:10.1016/S0301-9268(02)00218-8.

Kinoshita, O., 1995, Migration of igneous activities related to ridge subduction in Southwest Japan and the East Asian continental margin from the Mesozoic to the Paleogene: Tectonophysics, v. 245, n. 1–2, p. 25–35, doi:10.1016/0040-1951(94)00211-Q.

Kohn, M. J., and Spear, F., 2000, Retrograde net transfer reaction insurance for pressure-temperature estimates: Geology, v. 28, n. 12, p. 1127–1130, doi:10.1130/0091-7613(2000)28⟨1127:RNTRIF⟩2.0.CO;2.

Kovalenko, V. I., Yarmolyuk, V. V., Kovach, V. P., Kotov, A. B., Kozakov, I. K., Salnikova, E. B., and Larin, A. M., 2004, Isotopic provinces, mechanism of generation and sources of the continental crust in the Central Asian mobile belt: geological and isotopic evidence: Journal of Asian Earth Sciences, v. 23, n. 5, p. 605–627, doi:10.1016/S1367-9120(03)00130-5.

Kröner, S., Konopasek, J., Kröner, A., Passchier, C. W., Poller, U., Wingate, M. T. D., and Hofmann, K. H., 2004, U-Pb and Pb-Pb zircon ages for metamorphic rocks in the Kaoko Belt of Northwestern Namibia: A Palaeo- to Mesoproterozoic basement reworked during the Pan-African orogeny: South African Journal of Geology, v. 107, n. 3, p. 455–476, doi:10.2113/107.3.455.

Kröner, A., Windley, B. F., Badarch, G., Tomurtogoo, O., Hegner, E., Jahn, B. M., Gruschka, S., Khain, E. V., Demoux, A., and Wingate, M. T. D, 2007, Accretionary growth and crust formation in the Central Asian Orogenic Belt and comparison with the Arabian-Nubian Shield: Geological Society of America, Memoirs, v. 200, p. 181–210, doi:10.1130/2007.1200(11).

Lagabrielle, Y., Guivel, C., Maury, R. C., Bourgois, J., Fourcade, S., and Martin, H., 2000, Magmatic-tectonic effects of high thermal regime at the site of active ridge subduction: the Chile Triple Junction model: Tectonophysics, v. 326, n. 3–4, p. 255–268, doi:10.1016/S0040-1951(00)00124-4.

Laurent-Charvet, S., Charvet, J., Monie, P., and Shu, L., 2003, Late Paleozoic strike-slip shear zones in eastern central Asia (NW China): New structural and geochronological data: Tectonics, v. 22, 1009, 24 p., doi:10.1029/2001TC901047.

Leake, B. E., Woolet, A. R., Arps, C. E. S., Birch, W. D., Gilbert, M. C., Grice, J. D., Hawthorne, F. C., Kato, A., Kisch, H. J., Krivovichev, V. G., Linthout, K., Laird, J., Mandaring, J. A., Maresch, W. V., Nickel, E. H., Rock, N. C. N., Ungaretti, L., Whittaker, E. J. W., and Guo, Y. Z., 1997, Nomenclature of amphiboles: report of the subcommittee on amphiboles of the International Mineralogical Association, commission on new minerals and mineral names: American Mineralogist, n. 9–10, v. 82, p. 1019–1037.

Li, H. J., He, G. Q., Wu, T. R., and Wu, B., 2006, Confirmation of Altai-Mongolia microcontinent and its implications: Acta Petrologica Sinica, v. 22, n. 5, p. 1369–1379 (in Chinese with English abstract).

Li, H. Q., and Chen, F. W., 2004, Isotopic geochronology of regional mineralization in Xinjiang, NW China: Geological Publishing House, p. 19–58 (in Chinese with English abstract).

Li, T. D., Qi, Z. M., Xiao, S. L., and Wu, B. Q., 1996, New improvement of comparative study of geology and mineralization of Altai between China and Kazakhstan, *in* Thesis Volume of the Symposium of the 8th Five Year Plan of Geoscience for Contribution to 30th IGC: Chinese Geological Society, Metallurgical Industrial Publishing House, p. 256–259 (in Chinese).

Liu, X. J., Xu, J. F., Wang, S. Q., Hou, Q. Y., Bai, Z. H., and Lei, M., 2009, Geochemistry and dating of E-MORB type mafic rocks from Dalabute ophiolite in West Junggar, Xinjiang and geological implications: Acta Petrologica Sinica, v. 25, p. 1373–1389 (in Chinese with English abstract).

Long, X., Sun, M., Yuan, C., Xiao, W., Lin, S., Wu, F., Xia, X. and Cai, K., 2007, Detrital zircon age and Hf isotopic studies for metasedimentary rocks from the Chinese Altai: Implications for the Early Paleozoic tectonic evolution of the Central Asian Orogenic Belt: Tectonics, v. 26, TC5015, 20 p., doi:10.1029/2007TC002128.

Long, X., Sun, M., Yuan, C., Xiao, W., and Cai, K., 2008, Early Paleozoic sedimentary record of the Chinese Altai: Implications for its tectonic evolution: Sedimentary Geology, v. 208, n. 1–4, p. 88–100, doi:10.1016/j.sedgeo.2008.05.002.

Long, X., Yuan, C., Sun, M., Xiao, W., Zhao, G., Wang, Y., Cai, K., Xia, X., and Xie, L., 2010, Detrital zircon ages and Hf isotopes of the early Paleozoic flysch sequence in the Chinese Altai, NW China: New constrains on depositional age, provenance and tectonic evolution: Tectonophysics, v. 480, n. 1–4, p. 213–231, doi:10.1016/j.tecto.2009.10.013.

Ludwig, K. R., 2003, User's Manual for Isoplot 3.00: A Geochronological Toolkit for Microsoft Excel: Berkeley, Berkeley Geochronology Center, Special Publication N. 4a, 70 p.

Macpherson, C. G., and Hall, R., 2001, Tectonic setting of Eocene boninite magmatism in the Izu-Bonin-Mariana forearc: Earth and Planetary Science Letters, v. 186, n. 2, p. 215–230, doi:10.1016/S0012-821X(01)00248-5.

Morishita, T., Hara, K., Nakamura, K., Sawaguchi, T., Tamura, A., Arai, S., Okino, K., Takai, K., and Kumagai, H., 2009, Igneous, Alteration and Exhumation Processes Recorded in Abyssal Peridotites and Related Fault Rocks from an Oceanic Core Complex along the Central Indian Ridge: Journal of Petrology, v. 50, n. 7, p. 1299–1325, doi:10.1093/petrology/egp025.

Mossakovsky, A. A., Ruzhentsev, S. V., Samygin, S. G., and Kheraskova, T. N., 1993, Central Asian fold belt: geodynamic evolution and history of formation: Geotectonics, v. 6, p. 3–33 (in Russian).

Nakajima, T., 1994, The Ryoke plutonometamorphic belt: crustal section of the Cretaceous Eurasian continental margin: Lithos, v. 33, p. 51–66, doi:10.1016/0024-4937(94)90053-1.

Niu, H., Sato, H., Zhang, H., Ito, J., Nagao, T., Terada, K., and Zhang, Q., 2006a, Juxtaposition of adakite, boninite, high-TiO_2 and low-TiO_2 basalts in the Devonian southern Altay, Xinjiang, NW China: Journal of Asian Earth Sciences, v. 28, n. 4–6, p. 439–456, doi:10.1016/j.jseaes.2005.11.010.

Niu, H. C., Yu, X. Y., Xu, J. F., Shan, Q., Chen, F. R., Zhang, H. X., and Zheng, Z. P., 2006b, Late Paleozoic volcanism and associated metallogenesis in the Altay area, Xinjiang, China: Beijing, Geological Publishing House, p. 83–136 (in Chinese with English abstract).

Pitra, P., and Waal, S. A., 2001, High-temperature, low-pressure metamorphism and development of prograde symplectites, Marble Hall Fragment, Bushveld Complex (Southern Africa): Journal of Metamorphic Geology, v. 19, p. 311–325, doi:10.1046/j.0263-4929.2000.00313.x.

Prouteau, G., Scaillet, B., Pichavant, M., and Maury, R., 2001, Evidence for mantle metasomatism by hydrous silicic melts derived from subducted oceanic crust: Nature, v. 410, p. 197–200, doi:10.1038/35065583.

Santosh, M., and Kusky, T., 2010, Origin of paired high pressure-ultrahigh-temperature orogens: a ridge subduction and slab window model: Terra Nova, v. 22, p. 35–42, doi:10.1111/j.1365-3121.2009.00914.x.

Schiano, P., Clocchiatti, R., Shimizu, N., Maury, R. C., Jochum, K. P., and Hofmann, A. W., 1995, Hydrous, silica-rich melts in the sub-arc mantle and their relationship with erupted arc lavas: Nature, v. 377, p. 595–600, doi:10.1038/377595a0.

Schulz, B., Klemd, R., and Brätz, H., 2006, Host rock compositional controls on zircon trace element signatures in metabasites from the Austroalpine basement: Geochimica et Cosmochimica Acta, v. 70, p. 697–710 doi:10.1016/j.gca.2005.10.001.

Sengör, A. M. C., and Natal'in, B. A., 1996, Paleotectonics of Asia: fragments of a synthesis, *in* Yin, A., and Harrison, M., editors, The Tectonic Evolution of Asia: Cambridge, Cambridge University Press, p. 486–640.

Sengör, A. M. C., Natal'in, B. A., and Burtman, V. S., 1993, Evolution of the Altaid tectonic collage and Paleozoic crustal growth in Eurasia: Nature, v. 364, p. 299–307.

Simon, J. I., Vazquez, J. A., Renne, P. R., Schmitt, A. K., Bacon, C. R., and Reid, M. R., 2009, Accessory mineral U-Th-Pb ages and $^{40}Ar/^{39}Ar$ eruption chronology, and their bearing on rhyolitic magma evolution in the Pleistocene Coso volcanic field, California: Contributions to Mineralogy and Petrology, v. 158, p. 421–446, doi:10.1007/s00410-009-0390-9.

Sisson, V. B., and Pavlis, T. L., 1993, Geologic consequences of plate reorganization: An example from the Eocene Southern Alaska fore arc: Geology, v. 21, p. 913–916, doi:10.1130/0091-7613(1993)021⟨0913:GCOPRA⟩2.3.CO;2.

Sisson, V. B., Hollister, L. S., and Onstott, T. C., 1989, Petrologic and age constraints on the origin of a low-pressure/high-temperature metamorphic complex, Southern Alaska: Journal of Geophysical Research, v. 94, n. B4, p. 4392–4410, doi:10.1029/JB094iB04p04392.

Sisson, V. B., Pavlis, T. L., Roeske, S. M., and Thorkelson, D. J., 2003a, Introduction: An overview of ridge-trench interactions in modern and ancient settings, *in* Sisson, V. B., Roeske, S. M., and Pavlis, T. L., editors, Geology of a transpressional orogen developed during ridge-trench interaction along the North Pacific margin: Geological Society of America Special Papers, v. 371, p. 1–18, doi:10.1130/0-8137-2371-X.1.

Sisson, V. B., Poole, A. R., Harris, N. R., Burner, H. C., Pavlis, T. L., Copeland, P., Donelick, R. A., and McLelland, W. C., 2003b, Geochemical and geochronological constraints for genesis of a tonalite-trondhjemite suite and associated mafic intrusive rocks in the eastern Chugach Mountains, Alaska: A record of ridge-transform subduction, *in* Sisson, V. B., Roeske, S. M., and Pavlis, T. L., editors, Geology of a transpressional orogen developed during ridge-trench interaction along the North Pacific margin: Geological Society of America Special Papers, v. 371, p. 293–326, doi:10.1130/0-8137-2371-X.293.

Spear, F. S., 1991, On the interpretation of peak metamorphic temperatures in light of garnet diffusion during cooling: Journal of Metamorphic Geology, v. 9, p. 379–388, doi:10.1111/j.1525-1314.1991.tb00533.x.

Spear, F. S., and Florence, F. P., 1992, Thermobarometry in granulites: pitfalls and new approaches: Precambrian Research, v. 55, p. 209–241, doi:10.1016/0301-9268(92)90025-J.

Spear, F. S., Kohn, M. J., and Cheney, J. T., 1999, *P-T* paths from anatectic pelites: Contributions to Mineralogy and Petrology, v. 134, p. 17–32, doi:10.1007/s004100050466.

Sun, M., Long, X. P., Cai, K. D., Jiang, Y. D., Wang, P. Y., Yuan, C., Zhao, G. C., Xiao, W. J., and Wu, F. Y., 2009, Early Paleozoic ridge subduction in the Chinese Altai: Insight from the abrupt change in zircon Hf isotopic compositions: Science in China, Series D, v. 52, p. 1345–1358, doi:10.1007/s11430-009-0110-3.

Sun, M., Yuan, C., Xiao, W. J., Long, X. P., Xiao, X. P., Zhao, G. C., Lin, S. F., Wu, F. Y., and Kröner, A., 2008, Zircon U-Pb and Hf isotopic study of gneissic rocks from the Chinese Altai: progressive accretionary history in the early to middle Palaeozoic: Chemical Geology, v. 247, p. 352–383, doi:10.1016/j.chemgeo.2007.10.026.

Sun, S. S., and McDonough, W. F., 1989, Chemical and isotopic systematics of oceanic basalts: implicatons for mantle composition and processes, *in* Sanders, A. D., and Norry, M. J., editors, Magmatism in the Ocean Basins: Geological Society, London, Special Publication, v. 42, p. 313–345, doi:10.1144/GSL.SP.1989.042.01.19.

Tang, G. J., Wang, Q., Wyman, D. A., Li, Z. X., Zhao, Z. H., Jia, X. H., and Jiang, Z. Q., 2010, Ridge subduction and crustal growth in the Central Asian Orogenic Belt: Evidence from Late Carboniferous adakites and high-Mg diorites in the western Junggar region, northern Xinjiang (west China): Chemical Geology, v. 277, p. 281–300, doi:10.1016/j.chemgeo.2010.08.012.

Teng, L. S., Lee, C. T., Tsai, Y. B., and Hsiao, L. Y., 2000, Slab breakoff as a mechanism for flipping of subduction polarity in Taiwan: Geology, v. 28, p. 155–158, doi:10.1130/0091-7613(2000)28⟨155:SBAAMF⟩2.0.CO;2.

Thorkelson, D. J., 1996, Subduction of diverging plates and the principles of slab window formation: Tectonophysics, v. 255, p. 47–63, doi:10.1016/0040-1951(95)00106-9.

Tomkins, H. S., Powell, R., and Ellis, D. J., 2007, The pressure dependence of the zirconium-in-rutile thermometer: Journal of Metamorphic Geology, v. 25, p. 703–713, doi:10.1111/j.1525-1314.2007.00724.x.

Tong, Y., Wang, T., Hong, D. W., Dai, Y. J., Han, B. F., and Liu, X. M., 2007, Ages and origin of the early Devonian granites from the north part of Chinese Altai Mountains and its tectonic implications: Acta Petrologica Sinica, v. 23, p. 1933–1944 (in Chinese with English abstract).

Vavra, G., Schmid, R., and Gebauer, D., 1999, Internal morphology, habit and U-Th-Pb microanalysis of amphibolite-to-granulite facies zircons: geochronology of Ivrea zone (Southern Alps): Contributions to Mineralogy and Petrology, v. 134, p. 380–404, doi:10.1007/s004100050492.

Wang, F. Z., Yang, M. Z., and Zheng, J. P., 2002, Geochemical evidence of the basement assembled by island arc volcanic terranes in Junggar basin: Acta Petrologica et Mineralogica, v. 21, p. 1–10.

Wang, T., Hong, D. W., Jahn, B.-M., Tong, Y., Wang, Y. B., Hang, B. F., and Wang, X. X., 2006, Timing, Petrogenesis, and setting of Paleozoic synorogenic intrusions from the Altai Mountains, Northwest China: implications for the Tectonic evolution of an Accretionary orogen: Journal of Geology, v. 114, p. 735–751, doi:10.1086/507617.

Wang, Z. H., Sun, S., Li, J. L., Hou, Q. L., Qin, K. Z., Xiao, W. J., and Hao, J., 2003, Paleozoic tectonic evolution of the northern Xinjiang, China: Geochemical and geochronological constraints from the ophiolites: Tectonics, v. 22, p. 1014, doi:10.1029/2002TC001396.

Watson, E., Wark, D. A., and Thomas, J. B., 2006, Crystallization thermometers for zircon and rutile: Contributions to Mineralogy and Petrology, v. 151, p. 413–433, doi:10.1007/s00410-006-0068-5.

Wei, C. J., Clarke, G., Tian, W., and Qiu, L., 2007, Transition of metamorphic series from the kyanite- to andalusite-types in the Altai orogen, Xinjiang, China: Evidence from petrography and calculated KMnFMASH and KFMASH phase relations: Lithos, v. 96, p. 353–374, doi:10.1016/j.lithos.2006.11.004.

White, D. J., 2005, High-temperature, low-pressure metamorphism in the Kisseynew domain, Trans-Hudson orogen: crustal anatexis due to tectonic thickening: Canadian Journal of Earth Sciences, v. 42, p. 707–721, doi:10.1139/e04-087.

White, R. W., Powell, R. and Holland, T. J. B., 2001, Calculation of partial melting equilibria in the system Na_2O-CaO-K_2O-FeO-MgO-Al_2O_3-SiO_2-H_2O (NCKFMASH): Journal of Metamorphic Geology, v. 19, p. 139–153, doi:10.1046/j.0263-4929.2000.00303.x.

Wiedenbeck, M., Alle, P., Corfu, F., Griffin, W. L., Meier, M., Oberli, F., von Quadt, A., Roddick, J. C., and Spiegel, W., 1995, Three natural zircon standards for U-Th-Pb, Lu-Hf, trace element and REE analyses: Geostandards and Geoanalytical Research, v. 19, p. 1–23, doi:10.1111/j.1751-908X.1995.tb00147.x.

Windley, B. F., Kröner, A., Guo, J. H., Qu, G. S., Li, Y. Y., and Zhang, C., 2002, Neoproterozoic to Paleozoic geology of the Altai Orogen, NW China: new zircon age data and tectonic evolution: The Journal of Geology, v. 110, p. 719–737, doi:10.1086/342866.

Windley, B. F., Alexeiev, D., Xiao, W. J., Kröner, A., and Badarch, G., 2007, Tectonic models for accretion of the Central Asian Orogenic Belt: Journal of the Geological Society, London, v. 164, p. 31–47, doi:10.1144/0016-76492006-022.

Wong, K., Sun, M., Zhao, G. C., Yuan, C., and Xiao, W. J., 2010, Geochemical and geochronological studies of the Alegedayi Ophiolitic Complex and its implications on the evolution of the Chinese Altai: Gondwana Research, v. 18, p. 438–454, doi:10.1016/j.gr.2010.01.010.

Wu, C. M., Zhang, J., and Ren, L. D., 2004, Empirical Garnet-Biotite-Plagioclase-Quartz (GBPQ) Geobarometry in medium- to high-grade metapelites: Journal of Petrology, v. 45, p. 1907–1921, doi:10.1093/petrology/egh038.

Wu, Y. B., and Zheng, Y. F., 2004, Genesis of zircon and its constraints on interpretation of U-Pb age: Chinese Science Bulletin, v. 49, p. 1554–1569, doi:10.1360/04wd0130.

Xia, X. P., Sun, M., Zhao, G. C., Li, H. M., and Zhou, M. F., 2004, Spot zircon U-Pb isotope analysis by ICP-MS coupled with a frequency quintupled (213 nm) Nd-YAG laser system: Geochemical Journal, v. 38, p. 191–200.

Xiao, W. J., Windley, B. F., Hao, J., and Zhai, M. G., 2003, Accretion leading to collision and the Permian Solonker suture, Inner Mongolia, China: Termination of the central Asian orogenic belt: Tectonics, v. 22, p. 1069, doi:10.1029/2002TC001484.

Xiao, W. J., Windley, B. F., Badarch, G., Sun, S., Li, J., Qin, K., and Wang, Z., 2004, Palaeozoic accretionary and convergent tectonics of the southern Altaids: implications for the growth of Central Asia: Journal of the Geological Society, v. 161, p. 339–342, doi:10.1144/0016-764903-165.

Xiao, W. J., Windley, B. F., Yuan, C., Sun, M., Han, C. M., Lin, S. F., Chen, H. L., Yan, Q. R., Liu, D. Y., Qin, K. Z., Li, J. L., and Sun, S., 2009, Paleozoic multiple subduction-accretion processes of the southern Altaids: American Journal of Science, v. 309, p. 221–270, doi:10.2475/03.2009.02.

Xie, L. W., Zhang, Y. B., Zhang, H. H., Sun, J. F., and Wu, F. Y., 2008, *In situ* simultaneous determination of trace elements, U-Pb and Lu-Hf isotopes in zircon and baddeleyite: Chinese Science Bulletin, v. 53, p. 1565–1573, doi:10.1007/s11434-008-0086-y.

Xu, J. F., Mei, H. J., Yu, X. Y., Bai, Z. H., Niu, H. C., Chen, F. R., Zhen, Z. P., and Wang, Q., 2001, Adakites related to Subduction in the northern margin of Junggar arc for the Late Paleozoic: Products of slab melting: Chinese Science Bulletin, v. 46, p. 1313–1317.

Xu, J. F., Castillo, P. R., Chen, F. R., Niu, H. C., Yu, X. Y., and Zhen, Z. P., 2002, Geochemistry of late Paleozoic mafic igneous rocks from the Kuerti area, Xinjiang, northwest China: implications for backarc mantle evolution: Chemical Geology, v. 193, p. 137–154, doi:10.1016/S0009-2541(02)00265-6.

Yakubchuk, A., Cole, A., Seltmann, R., and Shatov, V., 2002, Tectonic setting, characteristics and regional exploration criteria for gold mineralization in Central Eurasia: the southern The Tien Shan province as a key example, *in* Goldfarb, R., and Nielsen, R. L., editors, Integrated methods for discovery: Global exploration in the twenty first century: Society of Economic Geologists, Special Publication 9, p. 177–201.

Yu, X., Niu, H. C., Xu, J., Chen, F., and Zheng, Z., 2000, On the fluid system of the paleozoic volcano-sedimentary basins and associated mineralization: Urumqi, Xinjiang, China, Chinese National 305 Project, p. 181 (in Chinese).

Yuan, C., Sun, M., Xiao, W. J., Li, X. H., Chen, H. L., Lin, S. F., Xia, X. P., and Long, X. P., 2007, Accretionary orogenesis of the Chinese Altai: Insights from Paleozoic granitoids: Chemical Geology, v. 242, p. 22–39, doi:10.1016/j.chemgeo.2007.02.013.

Zack, T., Moraes, R., and Kronz, A., 2004, Temperature dependence of Zr in rutile: empirical calibration of a rutile thermometer: Contributions to Mineralogy and Petrology, v. 148, p. 471–488, doi:10.1007/s00410-004-0617-8.

Zhang, C. G., Wei, C. J., and Qiu, L., 2004, Evolution of metamorphism and its geologic significance in Altaides, Xinjiang: Xinjiang Geology, v. 22, p. 16–23 (in Chinese with English abstract).

Zhang, C. G., Wei, C. J., Hou, R. J., Hou, L. S., and Bo, X. P., 2007, Phase equilibrium of low-pressure metamorphism in the Altaides, Xinjiang: Geology in China, v. 34, p. 34–41 (in Chinese with English abstract).

Zhang, H. X., Niu, H. C., Terada, K., Yu, X. Y., Sato, H., and Ito, J., 2003a, Zircon SHRIMP U-Pb dating on plagiogranite from Kuerti ophiolite in Altay, North Xinjiang: Chinese Science Bulletin, v. 48, p. 2231–2235.

Zhang, H. X., Niu, H. C., Yu, X. Y., Sato, H., Ito, J., and Shan, Q., 2003b, Geochemical characteristics of the Shaerbulake boninites and their tectonic significance, Fuyun County, northern Xinjiang, China: Geochemica, v. 32, p. 155–160 (in Chinese with English abstract).

Zhang, H. X., Niu, H. C., Sato, H., Yu, X. Y., Shan, Q., Zhang, B. Y., Ito, J. and Nagao, T., 2005, Late Paleozoic adakites and Nb-enriched basalts from northern Xinjiang: Evidence for the southward subduction of the Paleo-Asian Ocean: Island Arc, v. 14, p. 55–68, doi:10.1111/j.1440-1738.2004.00457.x.

Zhang, J. H., Wang, J. B., and Ding, R. F., 2000, Characteristics and U-Pb ages of zircon in metavolcanics from the Kangbutiebao Formation in the Altay region, Xinjiang: Regional Geology of China, v. 19, p. 281–287 (in Chinese).

Zheng, C., Takenori, K., Masaki, E., and Cuechun, X., 2007, CHIME monazite ages of metasediments from the Altai orogen in northwestern China: Devonian and Permian ages of metamorphism and their significance: The Island Arc, v. 16, p. 598–604, doi:10.1111/j.1440-1738.2007.00585.x.

Zheng, Y. F., Wu, Y. B., Zhao, Z. F., Zhang, S. B., Xu, P., and Wu, F. Y., 2005, Metamorphic effect on zircon Lu-Hf and U-Pb isotope systems in ultrahigh-pressure eclogite-facies metagranite and metabasite: Earth and Planetary Science Letters, v. 240, p. 378–400, doi:10.1016/j.epsl.2005.09.025.

Zhou, X. W., Wei, C., and Zhang, S. K., 2006, Implications of Micro-compositions of Garnet and Biotite from High-grade Meta-pelites: Progress in Natural Science, v. 16, p. 209–214, doi:10.1080/10020070612331343215.

Zhuang, Y., 1994, Tectonothermal evolution in space and time and orogenic process of Altaide, China: Changchun, Jilin Scientific and Technical Press, p. 402 (in Chinese with English abstract).